POLITECNICO DI TORINO

MASTER's Degree in NANOTECHNOLOGIES FOR ICTs

MASTER's Degree Thesis

Biosensor platform integrating organic electrochemical transistors for in-vitro continuous monitoring

Supervisors

Prof. Francesca FRASCELLA

Prof. Lucia NAPIONE

Prof. Simone Luigi MARASSO

Candidate

Diego BUSDRAGHI

JULY 2025

Abstract

In recent years, organic electrochemical transistors (OECTs) have attracted interest in the field of organic bioelectronics thanks to their distinctive properties. In these devices, the channel consists of an organic semiconducting polymer which is in contact with an electrolyte. The gate electrode, immersed in the electrolyte, regulates the conductivity of the channel. Biocompatibility, ease of fabrication, low cost, high ionic sensitivity and low-voltage operation are among the properties that make this class of devices suitable for a wide range of applications, such as biosensing, in-vitro monitoring, and wearable and implantable devices. The purpose of this thesis, which is part of the Cobalt project, is the fabrication of an OECT-based device capable of continuously monitoring the behaviour of the endothelial barrier. In-vitro monitoring, i.e. the possibility to analyse and study the behaviour of cell cultures outside of the living organisms, is of great importance because it allows a precise control of the experimental conditions, reduces the costs, and permits to study how cells respond to specifically induced stimuli. Moreover, the continuous collection of data over long periods of time is critical to understand the time evolution of certain biological processes and to identify any sudden changes in the behaviour of the biological sample under investigation. The endothelial barrier, situated on the surface of blood vessels, regulates the exchange of substances between the bloodstream and the adjacent tissues. The analysis of its behaviour is crucial to understand its permeability to certain therapeutic molecules and its implication in the dynamics of specific diseases. This work intends to give an overview of the device design and the processes involved in its fabrication. The device comprises a Top and a Bottom structure, each consisting of three branches. Each branch houses an OECT with a p-type poly(3,4-ethylenedioxythiophene) polystyrene sulfonate (PEDOT:PSS) channel. The three OECTs of the Bottom structure are placed at the base of three wells of a multi-well plate, while the three OECTs of the Top structure are inserted in three well inserts, at the bottom of which a layer of endothelial cells is grown. This design, that implements one OECT at each side of the membrane, opens the possibility for a wider set of analyses, depending on the input settings. The device fabrication starts with the creation of the OECTs gold electrodes through traditional subtractive photolithography techniques. The device is then cut with a CO2 laser and the Top and Bottom structures are bonded thanks to oxygen plasma bonding. Contacts between the device and an external ribbon cable are formed using a silver conductive paste and then passivated with an epoxy resin. The device is then electrically characterised and its biocompatibility is tested in an incubator.

Table of Contents

List of Figures

Acronyms

OECT	Organic electrochemical transistor.
FET	Field effect transistor.
CP	Conductive polymer.
HOMO	Highest occupied molecular orbital.
LUMO	Lowest unoccupied molecular orbital.
PPy	Polypyrrole.
EDOT	Ethylenedioxythiophene.
PEDOT	Poly(3,4-ethylenedioxythiophene).
PSS	Polysterene sulfonate.
MOS	Metal-oxide-semiconductor.
EDL	Electrochemical double-layer.
PDMS	Polydimethylsiloxane.
SMU	Source measure unit.
PBS	phosphate-buffered saline.
DMEM	Dulbecco's Modified Eagle Medium.
FBS	Fetal bovine serum.
NEAA	Non-essential amino acids.

TEER	Transepithelial electrical resistance.

List of Symbols

V_{GS}, V_G	Gate-source voltage
V_{DS}	Drain-source voltage
I_{DS}	Drain current
E_{V_G}	Electric field generated by the gate voltage
E_{V_D}	Electric field generated by the drain voltage
J	Current flux
q	Elementary charge
Q	Total charge
μ	Hole mobility
p	Hole density
p_0	Initial hole density
R	Resistor
C	Capacitance
C^*	Volumetric capacitance
τ_i	Ionic transient time
V_P	Pinch-off voltage
W	Width
L	Length
T	Thickness
g_m	OECT transconductance
V_{Th}	Threshold voltage
P	Laser power
ν	Laser frequency
E_{pulse}	Energy per laser pulse
$E_{density}$	Energy density of the laser
A_{spot}	Area of the laser spot
v_{scan}	Scanning speed of the laser head
d	Size of the laser spot

Chapter 1

Introduction

The activity presented in this thesis is part of the projects "D3 4 Health: Digital Driven Diagnostics, prognostics and therapeutics for sustainable Health care (Piano nazionale per gli investimenti complementari al PNRR, finanziato dall'Unione europea – NextGenerationEU)" and "COBALT - COmprehending human biological BArriers for precision medicine with digitaL and biological Twins (Programma Regionale Valle d'Aosta FESR 2021/2027)".
The activities reported in this work were performed at *ChiLab - Materials and Microsystems Laboratory* (Politecnico di Torino) in Chivasso and at *Istituto nazionale di ricerca metrologica* (INRiM) in Torino.
The aim of this thesis project is the development and fabrication of an OECT-based device capable of continuously monitoring the behavior of the membrane permeability of a layer of endothelial cells.
The thesis falls within the area of research of bioelectronics, a field that combines biology and electronics, which has drawn a lot of attention in recent years as many applications have emerged aimed at improving current diagnostic systems and providing a better understanding of how cells interact with the surrounding environment or how they respond to specific stimuli.
The biosensing platform (*Biological twin*) can be integrated with the biological cellular samples of different patients, presenting inflammatory diseases at various stages of progression, to monitor the barrier permeability variations in different pathological conditions. The data collected can be used to extract predictive algorithms (*Digital twin*) to address the need for innovative diagnostic and therapeutic techniques, which is the scope of the D34H and COBALT projects.

The device comprises six branches, each of which consists of a coupled top-bottom OECT pair, and is designed to be mounted on a multiwell plate. The lower section of each branch (referred to as Bottom OECT) is fixed to the basis of the corresponding well, while the upper section (referred to as Top OECT) is placed inside a transwell insert. At the bottom of the insert a semipermeable membrane is present on which a monolayer of cells can be grown. This specific configuration, consisting of a set of two coupled OECTs integrated in each well - one upon the cellular barrier, one below

it - allows to study and analyse the barrier with different approaches and techniques, depending on how the two separate OECTs are polarized.
The biosensor platform intends to provide a way for continuously monitoring the barrier under analysis, a feature that is of great importance if one wants to understand the dynamics of biological processes or monitor some key parameters over long periods of time. Indeed, biological mechanisms and reactions can have long characteristic timescales, so it would not be possible to have a thorough comprehension of their evolution with only discrete-time measurements.
With regard to the biological aspect, endothelial cells are present on the interior surface of blood and lymphatic vessels, forming the endothelium, a barrier that controls the exchange of substances and fluids between blood and tissues, thus being involved in several biological functions. The permeability of endothelial barriers can be modulated by various factors, such as mechanical stimuli or chemical signals, and its dysfunction is associated with different diseases. Therefore, studying the behaviour of the endothelial barrier permeability and understanding the mechanisms that regulate its function is crucial to develop new therapies to prevent and treat diseases related to its dysfunction.
In the next chapter, an excursus on the theoretical background regarding the thesis subject will be presented. In the subsequent chapters, the experimental activities and the obtained results will be introduced, followed by the conclusive chapter, where future perspectives are highlighted.

Chapter 2

Theoretical background

2.1 Organic electrochemical transistors

Since their invention in 1947 thanks to the work of Bardeen, Brattain, and Shockley, transistors have become a constitutive element in electronics. A transistor is a three-terminal device in which the output signal can be modulated through an input signal, and thus it may operate both as a switch or as an amplifier. In the former case, by varying the input signal it is possible to regulate the behaviour of the transistor between an On state, where a current flows between the output terminals, and an Off state, in which no output signal is present; in the latter case, instead, a weak input signal is used to control a larger output signal, leading to an amplification proportional to the gain of the transistor.
Field effect transistors (FETs) are among the most common types of transistors. They consist of three terminals called Gate, Source, and Drain. By varying the voltage signal applied between the gate and source terminals (V_{GS}) it is possible to modulate the current flowing in the channel (I_{DS}), provided that a voltage V_{DS} is applied between source and drain.

Since their invention, a lot of effort was put into the research of new possible types of transistor, trying to exploit the properties of different materials or device designs to have the most suitable features for each specific application.
The use of organic materials in transistors led to the development of a new class of devices, namely organic transistors. Organic electrochemical transistors (OECTs) belong to this class of transistors, as their channel consists of an organic semiconductor. They were first demonstrated by White et al. in 1984 [1].
As will be presented in the next sections, the OECT has drawn a lot of interest in bioelectronics, used in applications ranging from biosensors to neuromorphic computing, because of its compatibility with aqueous media and the ability to convert and amplify ionic and biological signals into an electronic output [2]. OECTs' operation is in fact based on the mixed conduction properties (ionic and electronic) of the material in the channel, allowing them to convert ionic fluxes in the electrolyte into electronic signals. Moreover, the intrinsic amplification of the ionic signals during

the ionic-to-electronic conversion makes them a valuable tool for biosensing, allowing the detection of weak biological signals [2].
Another peculiarity of OECTs is that the ion permeable channel endows these devices with a high volumetric capacitance as opposed to the thin interfacial region of standard FETs. As a consequence, large modulations in the drain current can be obtained with low working voltages. This prevents the risk of water electrolysis in aqueous samples and can preserve the integrity of biological molecules [3] [4].
Another advantage of organic transistors derives from the ease of fabrication, since organic materials can be deposited using simple solution-phase techniques.
With respect to their inorganic counterpart, OECTs are also easier to fabricate on flexible substrates thanks to the high-degree of flexibility of organic molecules. The flexible OECT biosensor is a promising technology for use in wearable or implantable medical devices.
Additionally, their intrinsic biocompatibility makes OECTs suitable for applications where interaction with biological systems, stimulation of cell growth, or promotion of tissue regeneration are needed [3].
Finally, the inherent tunability of organic molecules permits optimization of ionic and electronic transport and enables facile biofunctionalization [4].

2.2 Organic conductive polymers

Organic conductive polymers (CP) are an essential element in OECTs, whose operation principle is based on the possibility of this class of polymers to conduct electricity. Moreover, conductive polymers have other properties that make them appealing, such as simple synthesis and processing conditions, tunable conductivity, and flexibility [5]. CPs, as all polymers, are constituted by the repetition of single units, called monomers. In the case of organic polymers, the primary structure consists of a chain of carbon atoms, also called carbon backbone. Furthermore, conductive polymers are characterised by the presence of conjugated bonds, i.e. by the alternation of single and double bonds linking the carbon atoms of the backbone (Fig. 2.1) - this peculiarity includes them in the class of conjugated polymers -.

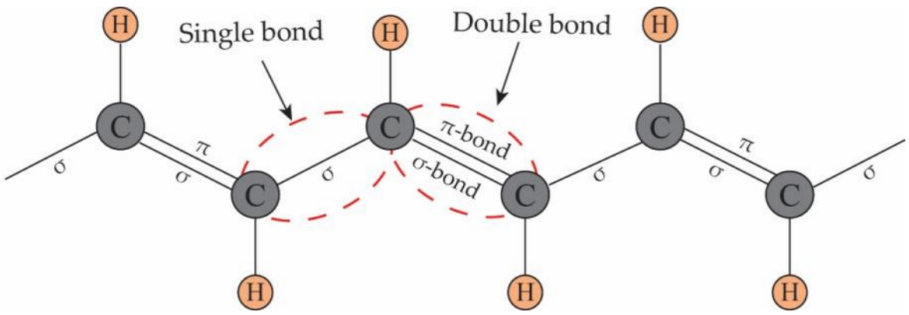

Figure 2.1: Conjugated double bonds in CPs. Reproduced by [5]

This specific bond conformation is responsible for their electrical properties. Single and double bonds both have a localized σ-bond, but the double bond also presents a localized π-bond. The alternation of single and double bonds allows for the delocalization of the π-electrons, that ultimately are responsible for the conductivity of conjugated polymers. To better visualize this condition, it is as if the π-bond that links the first and second atoms of the carbon backbone moves to the position in between the second and third carbon atoms, thus causing the π-bond between the third and fourth atoms to shift in turn towards the fourth and fifth ones (Fig. 2.2) [5].

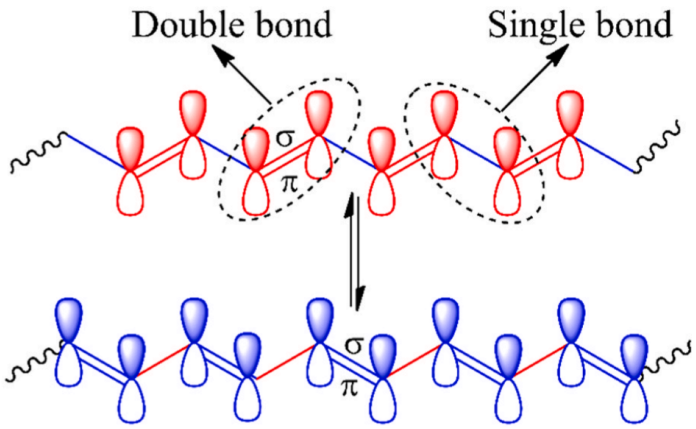

Figure 2.2: Visualization of π-electron delocalization in CPs. Reproduced by [6]

In other words, since the carbon backbone consists of a chain of adjacent sp_2 hybridized carbon atoms, all the p_z orbitals of each atom, which are orthogonal to the other three hybridized ones, combine in a single delocalized orbital where electrons are free to move along the chain.

However, the presence of conjugated bonds does not contribute to a high conductivity value; doping is necessary to obtain better results. The doping mechanism in CPs is different with respect to that in inorganic materials. Dopants are involved in redox processes, as they can extract electrons from the HOMO of the valence band (p-type doping, oxidation) or transfer electrons to the LUMO of the conduction band (n-type doping, reduction). In both cases, these oxidation/reduction processes create charge carriers - polarons, bipolarons, and solitons - whose movement across the polymer structure is responsible for the increase of CPs conductivity. Usually, p-type doping is preferred because the positive charge carriers that are created are more stable than their negative counterpart.

The mentioned polaron arises from the coupling between a localized charge and the local deformation of the polymer structure that it has induced. When instead two charges of the same sign bind together, causing a stronger distorsion in the backbone, a bipolaron is formed. For example, considering p-type doping in the case of polypyrrole (PPy, an organic polymer), when a dopant atom removes a π-electron from the polymer chain a hole is left behind. The hole electronic charge alters the

PPy structure from a benzenoid form to a quinoid one, thus creating a polaron. If further oxidation occurs, another electron is removed from the PPy backbone, with the consequent formation of doubly charged bipolaron (Fig. 2.3).

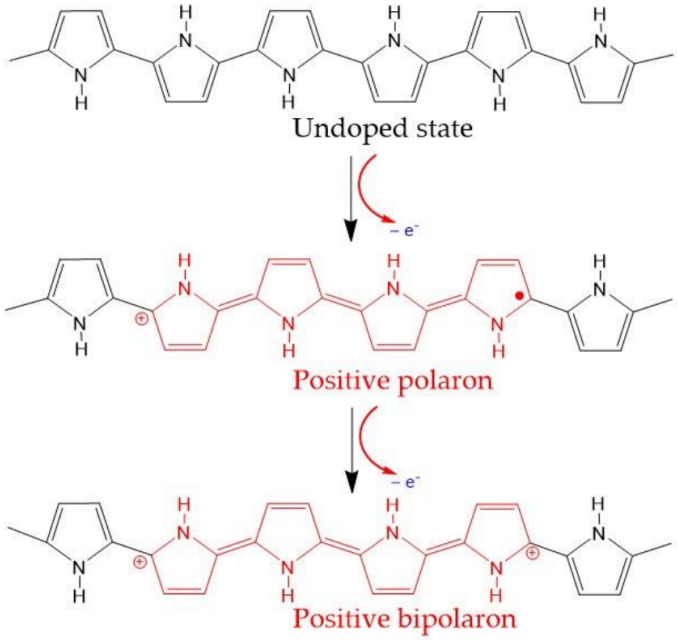

Figure 2.3: Illustration of chemical structures of undoped state (benzenoid structure), positive polaron and positive bipolaron (quinoid structure) in PPy. Reproduced by [5]

When dealing with degenerate CPs, i.e. polymers that at the ground state possess two identical geometrical structures with the same energy, another type of charge carrier may be present, a soliton. A soliton consists of a topological defect in the configuration of a degenerate polymer that separates two regions with the two opposite ground state structures. It has a certain mobility allowing it to be delocalized along the polymer backbone (Fig. 2.4) [5] [6].

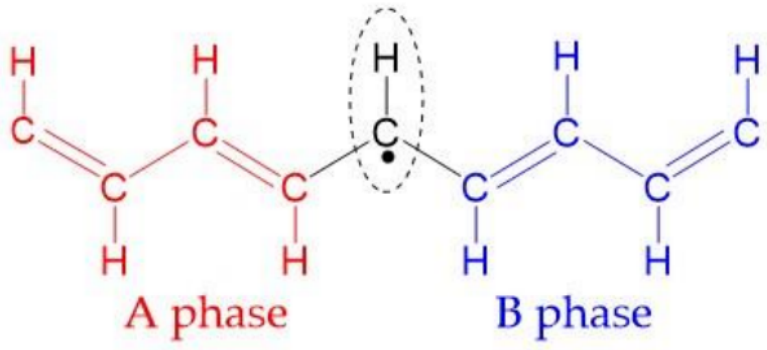

Figure 2.4: Illustration of the chemical structure of a neutral soliton in trans-polyacetylene chain. Reproduced by [5]

2.2.1 PEDOT:PSS

PEDOT:PSS is one of the most common conductive polymers used in OECTs. It consists of the combination of poly(3,4-ethylenedioxythiophene) (PEDOT) and polystyrene sulfonate (PSS) (Fig. 2.5). PEDOT is a hole-conductive conjugate

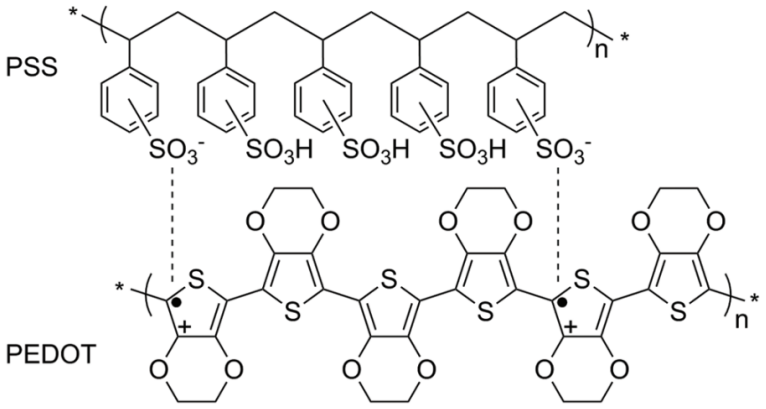

Figure 2.5: Chemical structure of PEDOT:PSS. Reproduced by [7]

polymer obtained by the oxidative polymerization of the EDOT monomer. PSS not only serves as counter-ion to electrostatically balance the positive charge of PEDOT chains - thanks to the negatively charged sulfonate groups - but also to make PEDOT:PSS soluble in water [7] [8]. Therefore, in presence of aqueous electrolytes, hydrated cations, when electrically addressed, are able to de-dope PEDOT:PSS by disrupting the electrostatic polaron $—SO_3^-$ bonds between the PEDOT backbone and PSS. As a consequence, PEDOT chains are distorted, hole transport pathways are interrupted, and therefore, the hole conductivity of the material is reduced (Fig. 2.6). This conductivity modulation mechanism is the principle of operation for PEDOT:PSS-based bioelectronic devices [8].

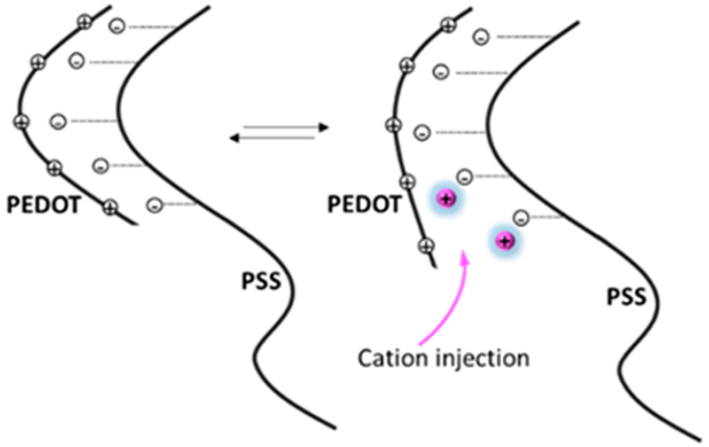

Figure 2.6: Schematic of PEDOT:PSS de-doping mechanism. Reproduced by [8]

Among the advantages of PEDOT:PSS there is its commercial availability in aqueous dispersions that permits the facile deposition of thin films using solution processing techniques, its high conductivity, good mechanical flexibility, long-term thermal stability and compatibility with biological environments thanks to its strong electrochemical stability [9] [4]. In general, it is quite simple to make PEDOT:PSS OECTs with transconductance in the range of mS and a response time in the range of tens of μs, which makes these devices attractive for a variety of applications. [4]

2.3 OECT operating principle

The OECT structure consists of a layer of organic semiconductive polymer deposited between the source and drain electrodes, forming the transistor channel, and a gate electrode immersed in an electrolyte that is in direct contact with the channel (Fig. 2.7). The operation of an OECT relies on the injection of ions from the electrolyte

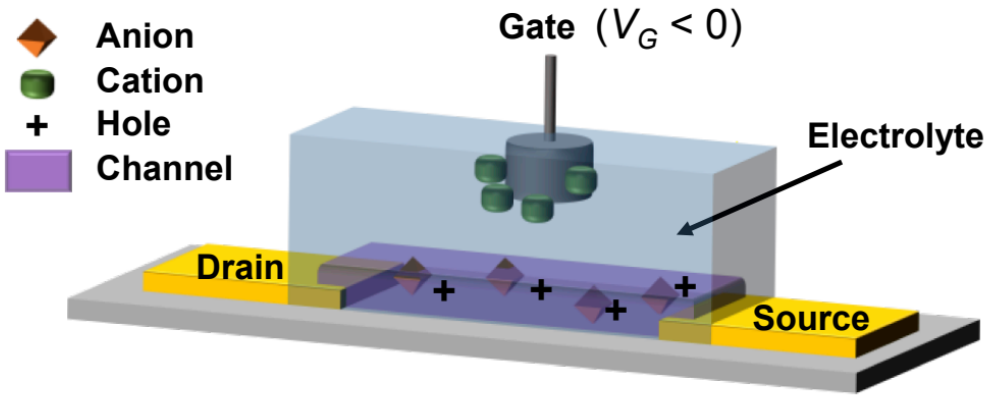

Figure 2.7: OECT structure. Reproduced by [10].

into the conductive polymer. The injected ions change the polymer's doping state and therefore its conductivity. The ion injection can be controlled by means of the gate voltage V_{GS} applied to the gate electrode and referenced to the source one. The drain to source voltage V_{DS} allows instead the flow of a current into the channel (I_{DS}) (Fig. 2.8). The I_{DS} current depends on the doping state of the channel. OECTs may have two operation modes, depletion and accumulation (Fig. 2.9), depending on the doping state of the channel material. In our case, the PEDOT:PSS channel OECT is an example of a depletion mode transistor. If no gate voltage V_{GS} is applied, a hole current flows and the device is in the ON state. When instead a positive voltage is applied at the gate electrode, the cations present in the electrolyte are injected into the organic polymer and are paired to the PSS anions, while holes are extracted at the drain electrode. Therefore, the PEDOT:PSS gets de-doped and the I_{DS} current is reduced accordingly (OFF state). This de-doping process is reversible, so when V_{GS} is reversed or removed, the previously injected cations leave the channel and PSS forms back the bonds with PEDOT oxidising it [2].

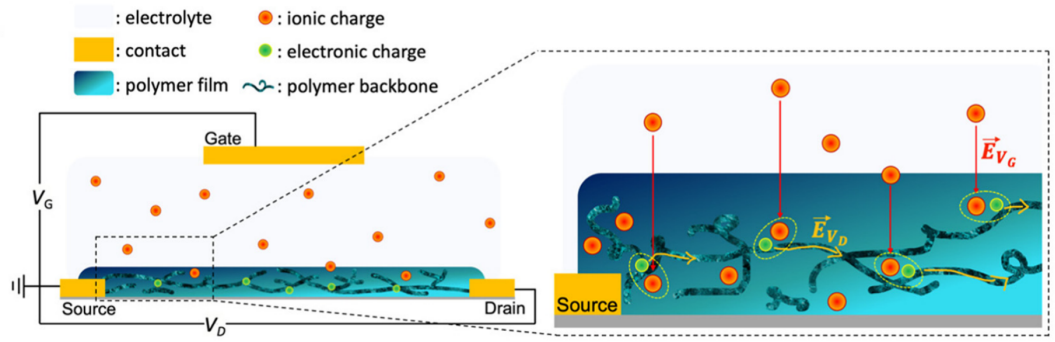

Figure 2.8: OECT operating principle. The electric field generated at the gate E_{V_G} moves the ions towards the polymer channel, while the voltage applied between source and drain (E_{V_D}) causes the electronic charges to flow through the channel generating a source-drain current. Reproduced by [2].

On the other hand, in accumulation mode OECTs the CP is undoped, thus the transistor is in the OFF state if no voltage is applied at the gate, since a small amount of charge carriers is present in the channel. The application of a gate voltage causes the injection of ions into the channel stabilising the carriers injected along the backbone. The electrostatic coupling between electronic and ionic charges increases the conductivity of the channel, switching the device from an OFF to an ON state [2].

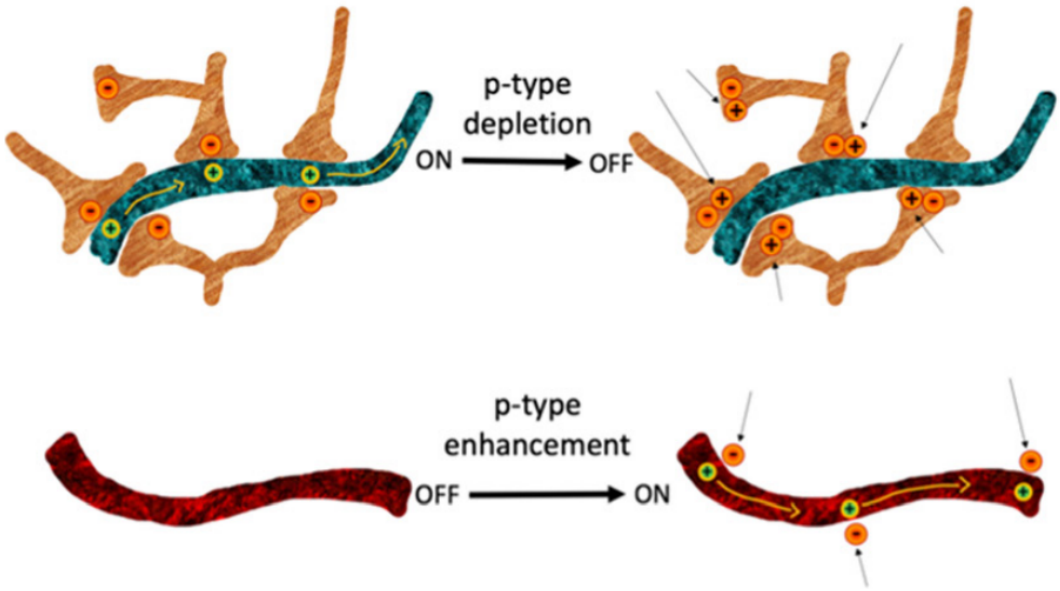

Figure 2.9: OECT operation modes. Upper picture shows a p-type depletion OECT where cations penetrating the channel deplete the holes by compensating with anionic species. The lower scheme illustrates a p-type accumulation OECT, in which the penetrating anions stabilise the holes. Reproduced by [2].

2.4 OECT device model

A model describing the OECT device behaviour was proposed in 2007 by Bernards and Malliaras [11]. In particular, the model describes the behaviour of a depletion mode OECT, which is the type of device used in this thesis project. Bernard's model divides an OECT into an electronic circuit and an ionic one (Fig. 2.10). The former accounts for hole transport in the organic semiconductor while the latter accounts for ion transport in the electrolyte.

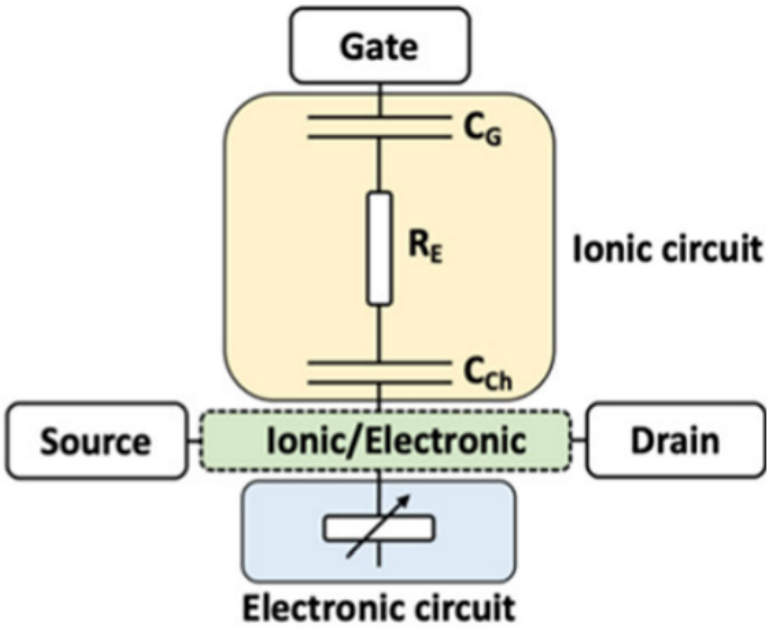

Figure 2.10: OECT device model, comprising an ionic and an electronic circuit. Reproduced by [2].

The electronic circuit models the hole transport between the source and drain electrodes through the Ohm's law:

$$J(x) = q\mu p(x)\frac{dV(x)}{dx} \tag{2.1}$$

where J is the current flux, q is the elementary charge, μ is the hole mobility, p is the hole density and $\frac{dV(x)}{dx}$ is the electric field.
As discussed, once a gate voltage V_{GS} is applied, cations present in the electrolyte are injected in the OECT channel, causing its de-doping. In fact, each cation that is injected compensates one acceptor ion (SO_3^- in PSS) and, as a consequence, one extracted hole is not replaced by injection at the drain. This mechanism preserves electrical neutrality in the organic film. With this considerations, it is possible to express the effective dopant density in a volume v of the semiconducting material as:

$$p = p_0\left(1 - \frac{Q}{qp_0v}\right) \tag{2.2}$$

where p_0 is the initial hole density in the organic polymer before the application of a gate voltage and Q is the total charge of the cations injected from the electrolyte. Concerning the ionic circuit, it consists of a resistor R_S and a capacitor C_D in series. The resistor is related to the conductivity of the electrolyte, while the capacitor considers the interface between the electrolyte and the organic semiconductor and the one between the gate electrode and the electrolyte. Under the assumption of a non-Faradaic regime of operation, the transient behaviour of the ionic circuit when a gate voltage is applied is the following:

$$Q(t) = Q_{SS}\left[1 - exp\left(-\frac{t}{\tau_i}\right)\right] \tag{2.3}$$

where $Q_{SS} = C_D \Delta V$ is the total charge flowing through the circuit, ΔV is the voltage applied across the electrolyte, and $\tau_i = C_D R_S$ is the ionic transit time. Considering the capacitance per unit area (c_D) it is possible to express C_D as $C_D = c_D A$ where A is the device area.
In order to know the spatial dependence of the effective dopant density in eq. 2.2 a section of the device as in Fig. 2.11 is considered.

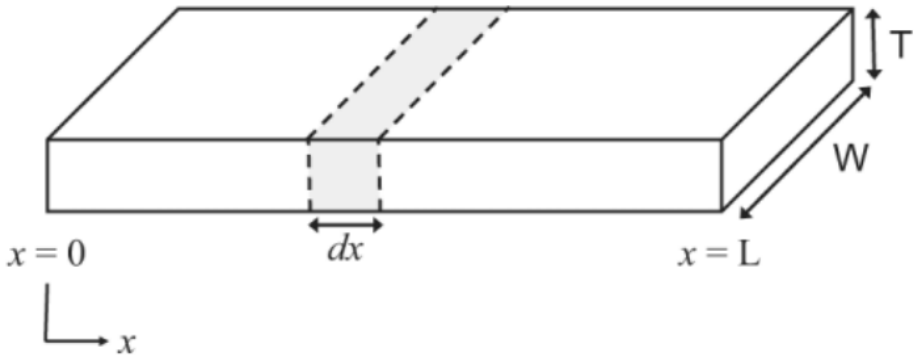

Figure 2.11: Device geometry used to analyse the OECT behaviour. Reproduced by [11].

The total charge present in a slice dx of the OECT can be expressed as:

$$Q(x) = c_D \cdot W \cdot dx(V_G - V(x)) \tag{2.4}$$

where V_G is the gate voltage, V(x) is the spatial profile of the voltage in the organic film and W is its width. Equation (2.4) couples the charge Q from the ionic circuit to the voltage V(x) at position x in the electronic circuit (Fig. 2.12).
The OECT steady-state characteristics can be obtained combining the previously considered equations:

$$J(x) = q\mu p_0 \left[1 - \frac{V_G - V(x)}{V_P}\right] \frac{dV(x)}{dx} \tag{2.5}$$

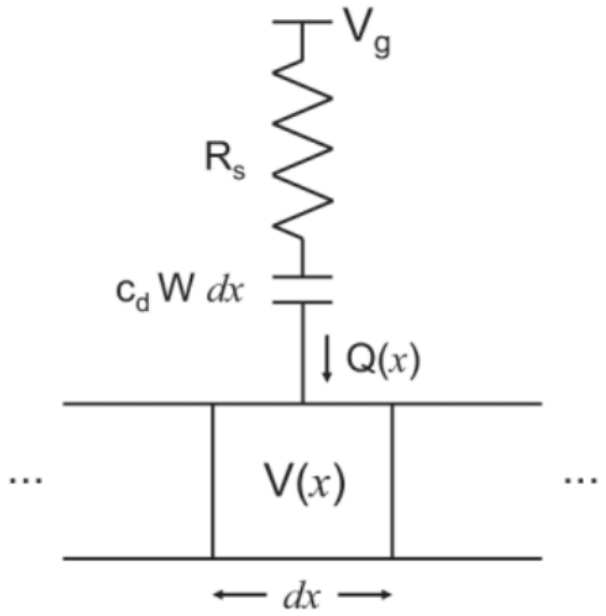

Figure 2.12: Coupling of the charge of the ionic circuit with the voltage considered in the electronic circuit. Reproduced by [11].

where $V_P = \frac{qp_0T}{c_D}$ is the pinch-off voltage. The equation can be solved explicitly for the various regimes of operation and provides a good fit for the experimental steady-state current-voltage characteristics of a PEDOT:PSS OECT at saturation. Moreover, Bernards model allows to predict the OECT tranconductance g_m in the saturation region as expressed in the following equation:

$$g_m = \frac{WT}{L}\mu C^* \left|(V_{Th} - V_G)\right| \tag{2.6}$$

where W and L are the channel dimensions, T is the organic film thickness, μ is the electronic charge carrier mobility, C^* is the volumetric capacitance, V_G is the gate voltage and V_{Th} is the threshold voltage [2].Transconductance, defined as the partial derivative of the drain current with respect to the gate voltage $\left(g_m = \frac{\partial I_{DS}}{\partial V_G}\right)$, is an important figure of merit of OECTs since it is linked to the the amplification factor and thus gives an idea of the efficiency of the device in transducing the signals. The large transconductance values typical of OECTs are attributed to the volumetric nature of their response [4].

This can be seen considering the OECT transconductance expression in eq.(2.6) which is similar to that of FETs, but in the case of OECTs the product of $T \cdot C^*$ is present instead of the capacitance per unit area of the MOS capacitor. This also highlights the fact that in OECTs the channel thickness is an important parameter that can be used to tune the device performance in terms of amplification [4]. However, the capacitance not only affects the OECT transconductance, but also influences the device operational speed. In the case of PEDOT:PSS channels the switching speed

of the device is limited by the ionic charge transport across the electrolyte and the organic film which is slower compared to the hole transport from source to drain. The response time, governed by the ionic circuit, can be derived by the RC time constant, so it is proportional to the device capacitance. Since the capacitance increases with the organic film thickness, a trade-off between gain and bandwidth must be found when optimizing the film thickness.

Another parameter worth mentioning when considering the performance of OECTs is the nature and the geometry of the gate electrode. In case of non-polarizable gate electrodes (Ag or AgCl), the applied gate voltage drops mainly across the electrolyte-channel interface, which is advantageous for a correct device operation. When dealing instead with polarizable gate electrodes, such as Au or Pt, an electrochemical double-layer capacitance is formed in series with the one of the channel. The EDL capacitance value needs to be larger in order to minimise the voltage drop across the gate-electrolyte interface. In this regard, having a gate electrode with a larger area compared to that of the channel is a possible option.

Chapter 3

Experimental

3.1 Device design

Considering that the device development and fabrication were the subject of study not only of this thesis work but also of a PhD thesis project, and part of a larger research program, the design of the biosensing platform was already provided,
The device overall view once mounted on the multi-well plate is shown in figures 3.1 and 3.2.

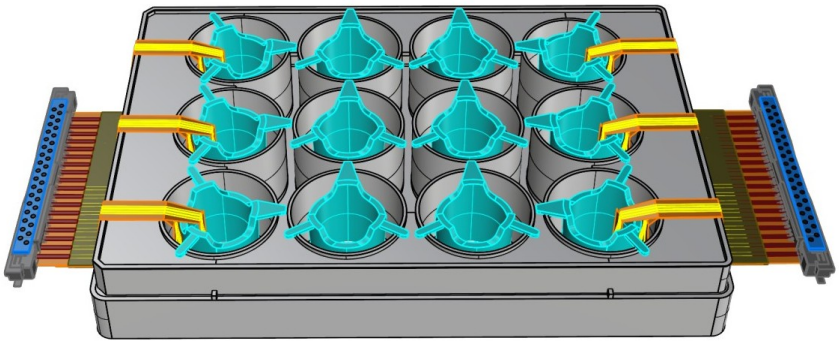

Figure 3.1: Horizontal view of the device when mounted on the multi-well plate

It is possible to notice:

- in *Grey* the multi-well plate;
- in *Light blue* the well inserts;
- in *Orange* the device Kapton® substrate;
- in *Yellow* the device gold electrodes.

More specifically, the biosensing platform consists of two separate units, placed on the opposite sides of the multi-well plate. Each of these units includes two bonded structures (Top and Bottom) that together form three coupled Top and Bottom OECT pairs, arranged in a branched layout. The Bottom structure (Fig. 3.3) comprises three branched OECTs, each of which is placed inside the three lateral

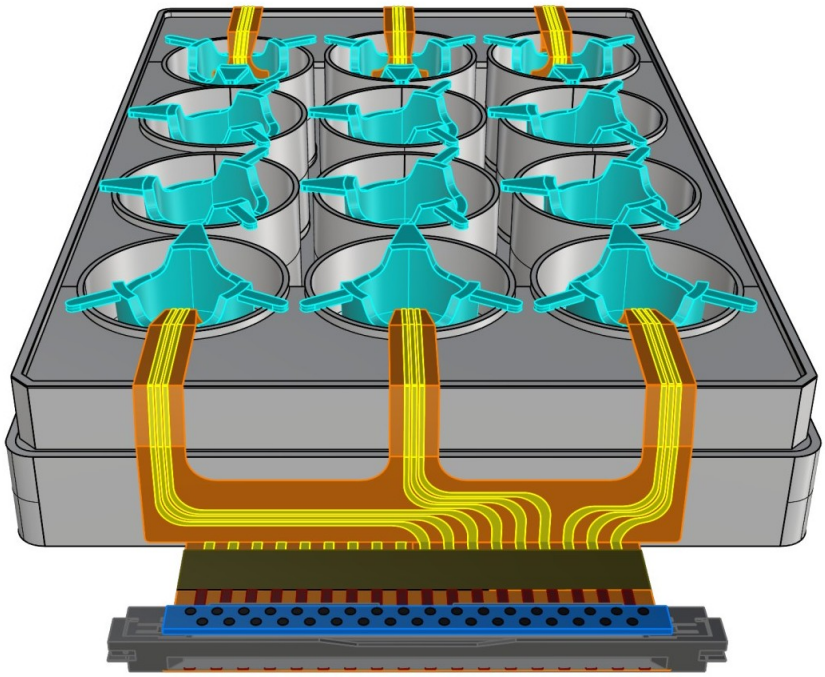

Figure 3.2: Vertical view of the device when mounted on the multi-well plate.

wells of the multi-well plate, as shown in Fig. 3.5.
On top of the Bottom structure is bonded the Top structure (Fig. 3.4), which includes as well three branched OECTs. These are inserted in the three well inserts that are found inside the three wells where the Bottom OECTs are, as shown in Fig. 3.6.

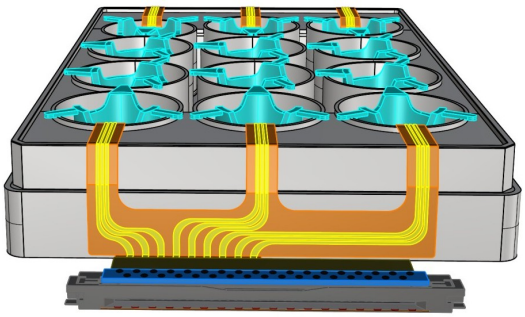

Figure 3.3: Bottom structure mounted on the multi-well plate. The gold electrodes are placed on the left.

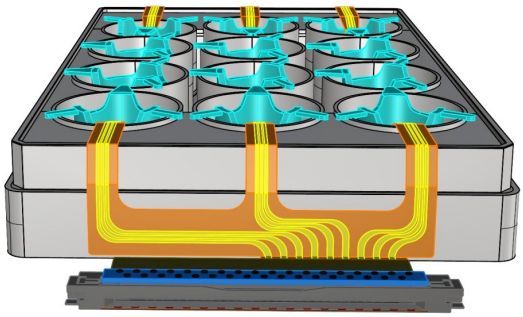

Figure 3.4: Top structure mounted on the multi-well plate. The gold electrodes are placed on the right.

Overall, when the device is assembled, each of the six lateral wells where the OECTs are found appears as depicted in Fig. 3.7. In particular, the device design requires the Bottom OECT to be placed underneath the well insert and the Top OECT to be placed inside it. On the bottom side of the well insert a layer of cells is grown, represented by the pink dots. If endothelial cells are deposited, this layer mimics an endothelial membrane, whose permeability behaviour can be analysed, and is the object of study of this device.

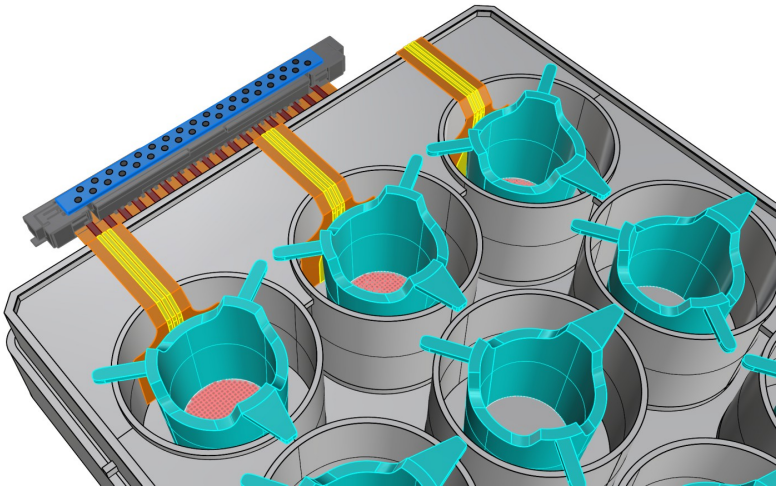

Figure 3.5: View of the Bottom structure OECTs inserted inside the lateral wells of the multi-well plate.

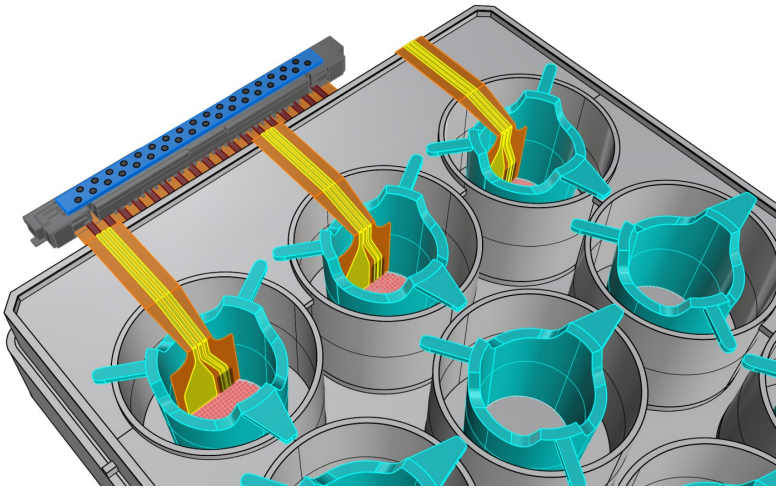

Figure 3.6: View of the Top structure OECTs placed inside the well inserts of the multi-well plate.

The black rectangles represent the PEDOT:PSS channels deposited between the source and drain electrodes of both Top and Bottom OECTs.

Concerning the electrodes, their design is shown in Fig. 3.8.
The terminal part of the electrodes, at the end of each branch, is the one devoted to biosensing, as it is immersed in the electrolyte. A close-up view is shown in Fig. 3.9. The gate electrode is the larger one, so that an efficient gating can be obtained. Indeed, when dealing with gold electrodes, which are polarizable, the area of the gate must be larger than that of the channel, otherwise a large portion of the gate voltage drops across the electrochemical double-layer capacitance that is formed at the interface with the electrolyte [4] [2].
The black square between the source and drain electrodes is the PEDOT:PSS channel.

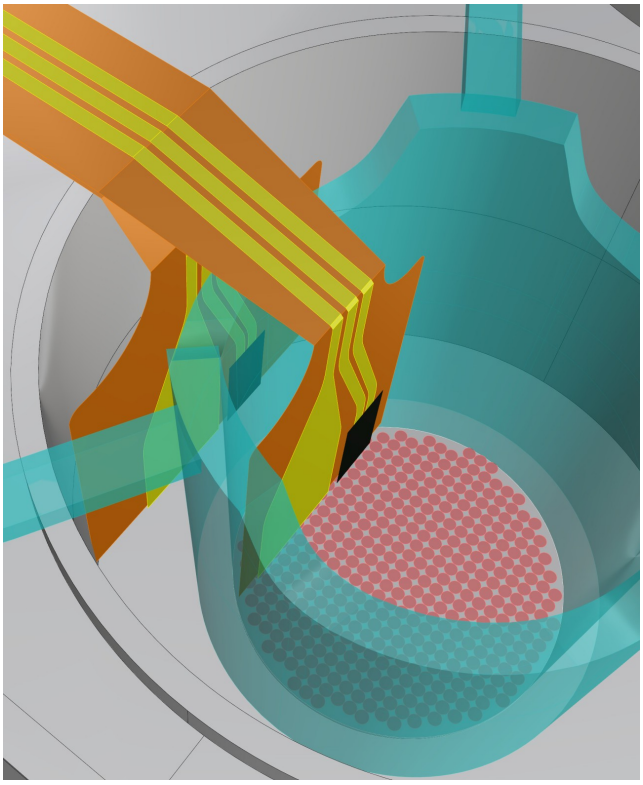

Figure 3.7: Close-up view of a well once the device is assembled.

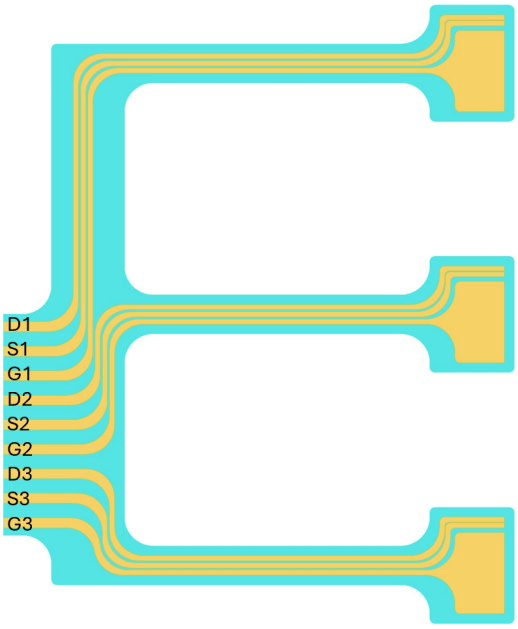

Figure 3.8: Gold electrodes geometry of the Top structure. D = drain, S = source, G = gate. 1,2 and 3 refer respectively to first, second and third OECT.

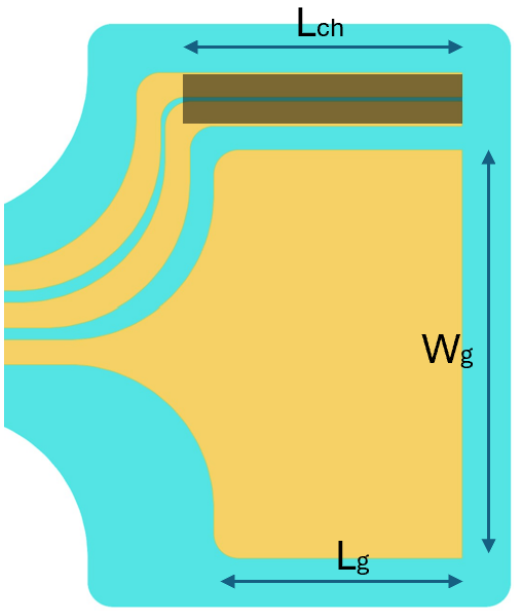

Figure 3.9: Terminal parts of the electrodes devoted to biosensing. PEDOT:PSS channel: length (L_{ch}) = $6mm$, width (W_{ch}) $\simeq$ $100\mu m$ i.e. the narrow separation between source and drain electrodes; gate electrode: length (L_g) = $8.4mm$, width (W_g) = $5mm$.

The electrodes' ends at the opposite side with respect to the branches, shown in Fig. 3.10, are instead the gold pads that will be connected to the wires of the ribbon cable. The process involved in the formation of the connections is presented in the next section.

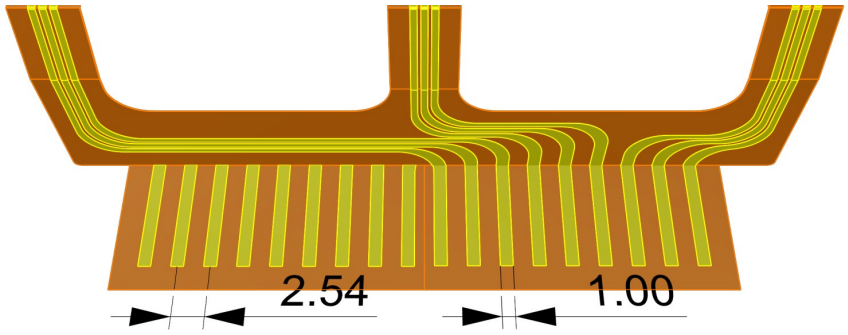

Figure 3.10: Gold electrodes' ends that are involved in the connection with the ribbon cable. The gold tracks are 1 *mm* wide. The pitch is 2.54 *mm*.

The gold tracks are 1 *mm* wide. Concerning the pitch, it is shown to be 2.54 *mm*, which is exactly twice the pitch of the 37-way ribbon cable ([12]) used for the connections. This means that only one way (the single electrical wire composing the cable) out of every two will be used for the electrical connections. Indeed, each of the two units at the two sides of the multi-well plate requires 18 connections, 9 for the Top structure and 9 for the Bottom one. Therefore, a 37-way ribbon cable can be adopted using only one way every two.
The ribbon cable is then connected to a 37-way D-Sub female connector [13], as represented in Fig. 3.11. The female D-sub connector is then connected to the

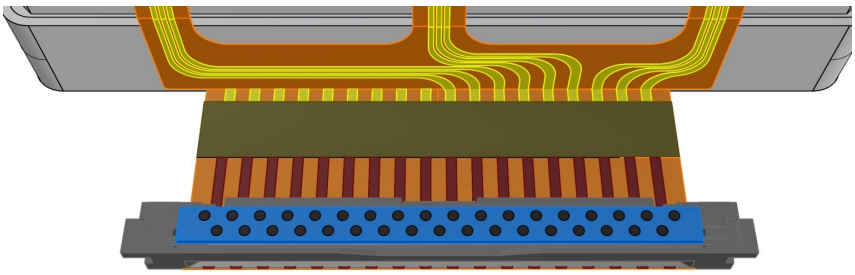

Figure 3.11: Graphical illustration of the electrical connection between the gold electrodes and the ribbon cable. The latter is then connected to a D-sub female connector. The grey rectangle between the ribbon cable and the gold electrodes represents a PDMS guiding structure that favours the contact formation, as it will be explained in the following sections.

corresponding male D-sub connector [14], that in turn connects the device to the source-measure unit (SMU). This setup, that splits the connection of the device to the SMU by means of the D-sub connectors, not only facilitates the handling and the transport of the two separated parts (the multi-well plate and the SMU), but also allows to divide the part that is supposed to stay in the incubator during the

analysis from the SMU, that instead does not need to be placed inside the incubator. A close-up view of the connections with the ribbon cable and the D-sub connector is depicted in Fig. 3.12.

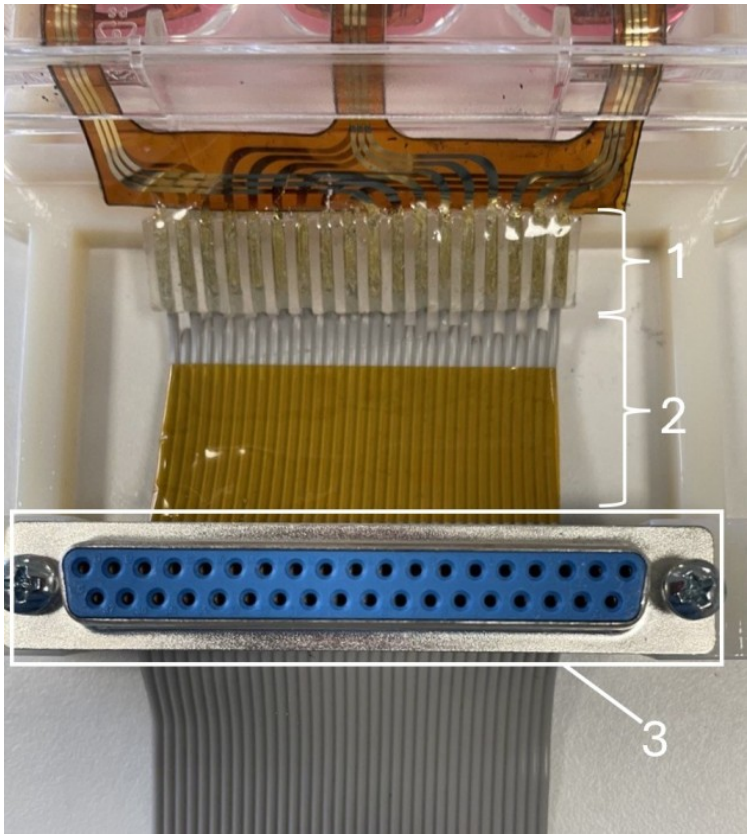

Figure 3.12: Final result of the electrical connections.
1. PDMS guiding structure that favours the formation of the contacts between the device electrodes and the ribbon cable.
2. Ribbon cable.
3. D-sub female connector.

3.1.1 Alternative design

An alternative version of the device layout was also designed. The idea of the new design came up after the creation of the PDMS guide structure for contacts creation. This structure provides the needed mechanical stability and allows the different branched OECTs to be assembled separately one from the other, without the need for them to be part of a single structure (either Top or Bottom). Thanks to this peculiarity, the bonding of the Top and Bottom structure is not needed anymore, and the same goes for their precise alignment.
Moreover, the new design also considers the spatial enlargement of the wires of the ribbon cable, thus allowing not to comply with the need of a precise pitch between the different gold pads. This permits the different electrodes to be more separated, reducing the risk of creating short circuits when forming the connections.
Figures 3.13, 3.14, 3.15 and 3.16 show the single OECTs as mounted on the multi-well

plate. As mentioned, each branch containing an OECT is separated from the others.

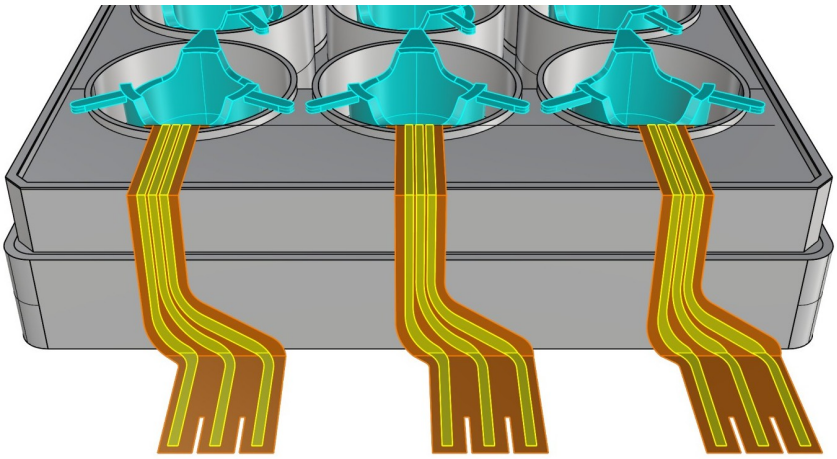

Figure 3.13: View of the three single Bottom OECTs. The three transistors are not part of the same structure as in the previous design.

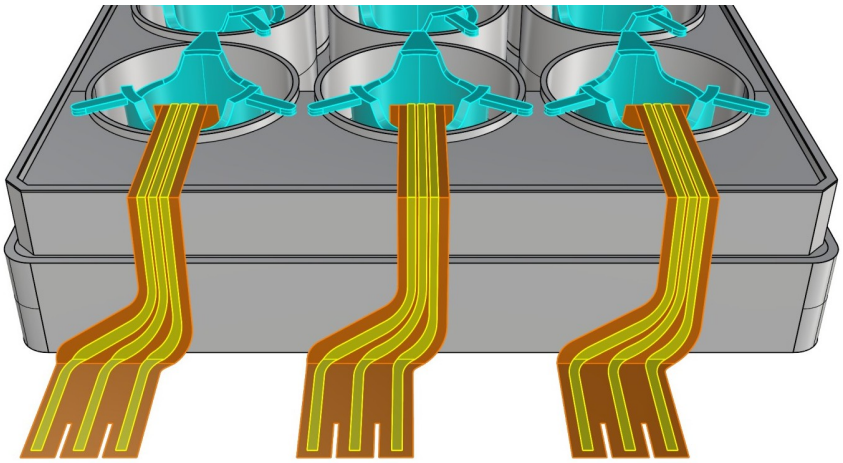

Figure 3.14: View of the three single Top OECTs. The three transistors are not part of the same structure as in the previous design.

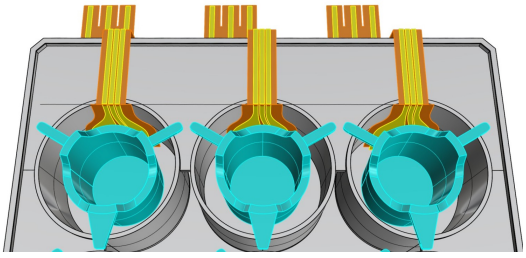

Figure 3.15: Bottom OECTs inserted in the three lateral wells.

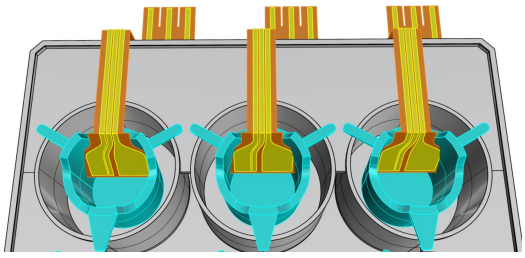

Figure 3.16: Top OECTs placed inside the well inserts.

The assembled device is illustrated in Fig. 3.17. The final parts of the ribbon cable ways are enlarged and connected to the gold pads of the OECTs. The other side of the cable is instead left intact and is connected to the D-sub connector, maintaining

the 2.54 *mm* pitch (as already mentioned, the connector and cable pitch is 1.27 *mm* but only one way every two is used, therefore the device pitch is doubled).

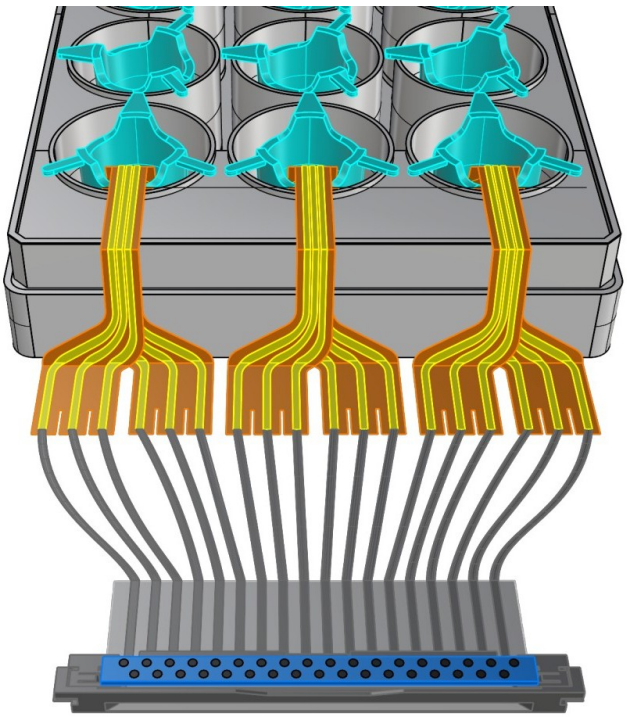

Figure 3.17: Overall view of the device design with all the OECTs mounted. The *grey* wires represent the ribbon cable ways that connect the device to the D-sub connector.

The final version of the device layout is shown in Fig. 3.18.

Figure 3.18: Final version of the device.

3.2 Device fabrication: materials and methods

3.2.1 Kapton

The substrate of the device, on which the gold electrodes are deposited, is a Kapton sheet [15]. Kapton is a polyimide film that was invented by DuPont. Its use in bioelectronics is due to its properties.
Kapton has a large temperature stability that allows it to operate at up to 400 C°.
It is used as an electrical insulator because of its dielectric properties.
Its flexibility is ideal for this application since it allows it to conform to the multi-well plate.
Moreover, Kapton is chemically resistant, so it can undergo sterilisation processes and does not degrade in biological environments.
Its biocompatibility makes it suitable for the study of cells' behaviour.
Finally, it is compatible with common microfabrication techniques, such as photolithography.

3.2.2 PDMS: properties and preparation

3.2.2.1 PDMS properties

Polydimethylsiloxane (PDMS) is an elastomer that has found large use in biomedical applications because of its properties. PDMS is biocompatible, so it is well-suited in applications in which the interface with biological environment is involved.
Moreover, PDMS is chemically inert, thermally stable, permeable to gases and simple to handle.
Mechanically speaking, it is flexible, which is a very important property for our application, since it needs to be deposited on a flexible Kapton substrate that has to bend and adhere to the wells and inserts of the multiwell plate. In this regard, PDMS has a hyperelastic behaviour [16], meaning that it can undergo large deformations before rupture.
Furthermore, PDMS is optically transparent, enabling observation through it if needed.
PDMS can work as a thermal and electrical insulator, so it can be used to protect some components from environmental factors in a large temperature range, up to 200 C° [16].
Finally, the possibility of being processed with low cost soft-lithography techniques, such as replica molding, has contributed to the popularity of PDMS in the field of biomedical applications.

3.2.2.2 PDMS preparation

PDMS was prepared using a Sylgard® 184 Silicone Elastomer Kit (Fig. 3.19) [17] that contains both the monomer and the curing agent. The main steps involved in the preparation are listed below:

1. First, the elastomer base and the curing agent are mixed in a 10:1 weight ratio;
2. the mixture is then stirred for about a minute with a laboratory spatula;
3. the mixture is put in a vacuum pump for about 15 minutes in order to remove the air bubbles created during the stirring process;
4. once PDMS has undergone the vacuum step, it is ready to be used, it can be spin-coated or cast in a master mold;
5. in order to be cured, PDMS is put in a Memmert laboratory oven at 100 C° for an hour.

Figure 3.19: Sylgard® 184 Silicone Elastomer Kit used to prepare PDMS

3.2.3 PDMS soft-lithography: replica molding

Among the several soft-lithographic techniques used in microfabrication that involve the use of PDMS, replica molding was chosen for our application.
The PDMS supporting structure used to facilitate the formation of the contacts, which will be discussed in the next chapter, is obtained by replica molding.
Replica molding is a procedure that allows the duplication of three-dimensional features in a single step.
It consists in the casting of a liquid elastomer (in this case PDMS) inside a master, thus conforming to its surface [18]. Once the elastomer has hardened, it is detached and presents the desired three-dimensional pattern. A schematic illustration of replica molding with PDMS is shown in Fig. 3.20.
The master mold used in this work has been 3D-printed; a CAD version of the mold is shown in Fig. 3.21. Further details on the purpose of the structure will be provided in the next chapter.
Once the mold has been adequately prepared, replica molding requires PDMS to be cast inside it. A toothpick was used to facilitate the deposition of small amounts of

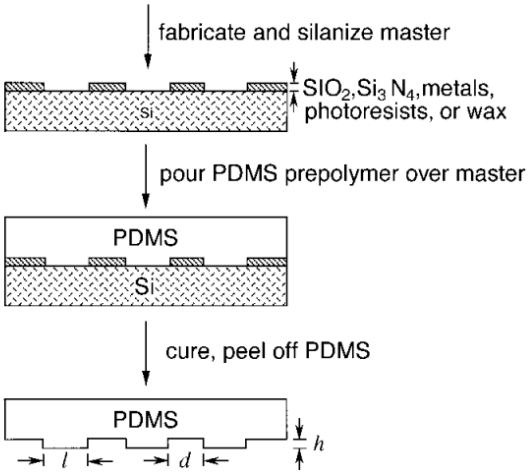

Figure 3.20: Schematic illustration of replica molding with PDMS poured on a master. Reproduced by [18]

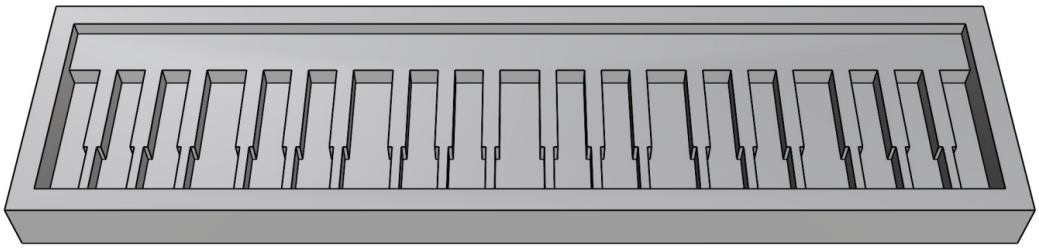

Figure 3.21: CAD version of the mold structure used for replica molding.

PDMS in the narrower features of the mold.
Air bubbles can be formed during casting. To remove them, the system can be placed under vacuum conditions for few minutes.
PDMS is then cured in an oven at 100 C° for an hour. Afterwards, the obtained PDMS structure is carefully detached from the mold by prying the edges of the structure with a laboratory spatula, paying attention not to ruin the PDMS. To favour the detachment, isopropyl alcohol is periodically poured with a Pasteur pipette.

3.2.4 PDMS spin-coating

The device fabrication requires the deposition of a very thin layer of PDMS on the Kapton substrate. This is done through spin-coating using a SPS Spin150 spin coater (Fig. 3.22). Spin-coating is a deposition technique that allows the deposition of thin layers of material across a flat substrate. In our case, the substrate is fixed to a silicon wafer, so that it can be secured to the wafer vacuum chuck of the spin coater. PDMS is then poured on the substrate, which is then rotated. The centrifugal force caused by the rotation of the wafer spreads and thins the PDMS. The spinning parameters, such as rotational speed and spinning time, are chosen in order to obtain the desired film thickness and depend on the material properties.

Figure 3.22: SPS Spin150 spin coater.

A schematic illustration of PDMS spin-coating is shown in Fig. 3.23.

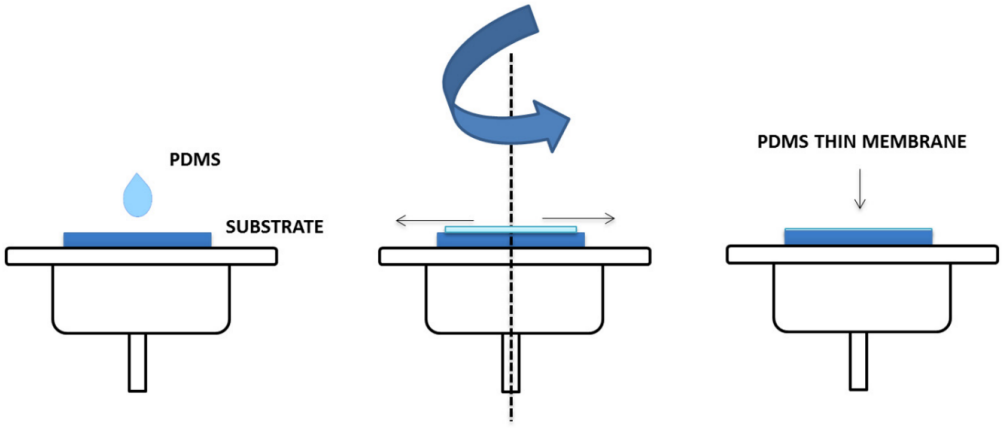

Figure 3.23: Schematic of PDMS spin-coating process. Reproduced by [19].

3.2.5 Profilometry

To measure the PDMS thickness obtained with different spinning parameters a profilometric analysis was performed. Profilometry is a technique used to extract topological data from a surface [20].
A Tencor P-17 stylus profiler was used for our analysis (Fig. 3.24).
Stylus profilometers use a probe that phisically moves along the sample to acquire the surface height. A feedback loop monitors the force from the sample pushing up against the probe and keeps the arm with a specific torque value on it. The

Figure 3.24: Tencor P-17 stylus profiler used for the profilometric analysis.

changes in the z position of the arm holder are then used to reconstruct the surface morphology.

The tip of stylus profilometers is in direct contact with the sample, so it can be destructive to some surfaces. In addition, the tip size and shape affect the resolution of the measures. This is not an issue for the analysis intended for this work, since profilometry is used to measure the step height of the samples, and precise surface morphology is not required.

A schematic of a stylus profilometer is shown in Fig. 3.25.

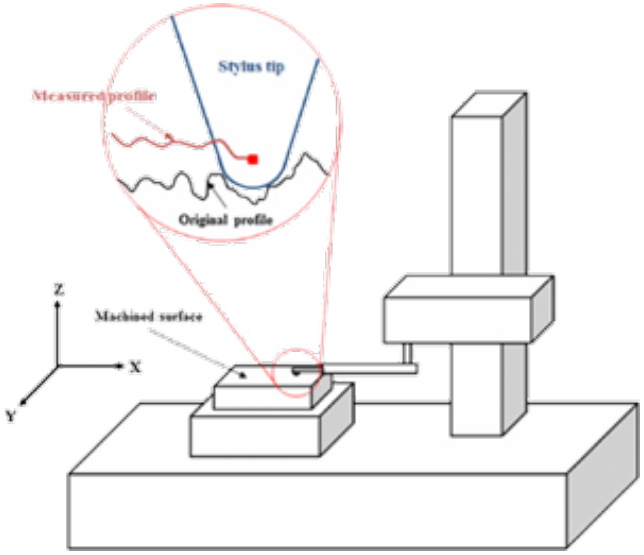

Figure 3.25: Schematic of the operation principle of a stylus profilometer. Reproduced by [20].

3.2.6 Laser cut

The cut of the Kapton substrates is performed using a Microla Laser Slider (Fig. 3.26).

Figure 3.26: Microla Laser Slider used for laser cutting.

The Microla Laser Slider is a CO_2 laser marker used for the incision of different substrates.
The more relevant technical specifications are reported here below:

- **Laser source**: CO_2
- **Wavelength**: 10.6 μm
- **Power**: 30 W
- **Frequency range**: 10 Hz - 25 kHz
- **Spot size**: 270 μm (with F-Theta Lens 100)
- **Working area**: 75mm $\times$ 75 mm (with F-Theta Lens 100)

The laser slider enables the setting of the laser parameters to adapt the cut to the material properties of the substrate that has to be incised. The main parameters are:

- the power of the laser, which is expressed as a percentage of the maximum laser power (30 W in our case). It is a measure of the amount of energy that is delivered to the material per unit time;
- the scan speed, which represents the speed at which the laser head moves across the substrate. A faster scanning implies that the laser will spend on average less time on a certain spot;

- the laser frequency, expressed in Hz, indicates the number of laser pulses per second. This value can be set between 10 Hz and 25 kHz. For a given power, a higher frequency corresponds to a lower energy per pulse;
- the number of repetitions, representing how many times the laser has to repeat the pattern of the cut.

The combination of these parameters together with the laser spot size, i.e. the diameter of the laser beam on the substrate, affects the dose of energy delivered to each point of the material. Indeed, considering the energy of a pulsed laser the energy per pulse can be obtained as:

$$E_{pulse} = \frac{P}{\nu} \tag{3.1}$$

where P and ν are respectively the power and the frequency of the laser.
The energy density can be calculated as:

$$E_{density} \propto \frac{E_{pulse}}{A_{spot}} \cdot PulseOverlap \tag{3.2}$$

where A_{spot} is the area of the laser spot, which is dependent on the spot size, and $PulseOverlap$ is a quantity that takes into account the overlap between two consecutive laser pulses. It can be expressed as [21]:

$$PulseOverlap = 1 - \frac{v_{scan}}{d \cdot \nu} \tag{3.3}$$

where v_{scan} is the scanning speed and d is the laser spot size. Therefore, the overlap of the different laser pulses depends on the scanning speed, laser frequency, and laser spot size. If the scanning speed is too large, the $PulseOverlap$ is negative, which essentially implies that a gap between two consecutive laser spots is formed.

3.2.7 Oxygen plasma bonding

Oxygen plasma bonding was performed at ChiLab laboratory in Chivasso using a Diener Atto plasma system (shown in Fig. 3.27) to bond the device Top and Bottom structures one to the other, since it strengthens the PDMS adhesion to PDMS itself. Indeed, when PDMS is treated with an oxygen plasma, reactive chemical groups are generated on the surface, allowing for the formation of strong covalent bonds.
More specifically, the surface activation induced by the plasma treatment causes the terminal methyl groups ($–CH_3$) to be replaced by silanol groups ($–Si–OH$). These can bond with the silanol groups that are present on the other PDMS activated surface thus forming covalent siloxane bonds ($Si–O–Si$), after the loss of a water molecule [22] [23].
The surface activation of PDMS is illustrated in Fig. 3.28 and 3.29.

Figure 3.27: Diener Atto plasma system used at ChiLab laboratory to perform oxygen plasma treatment.

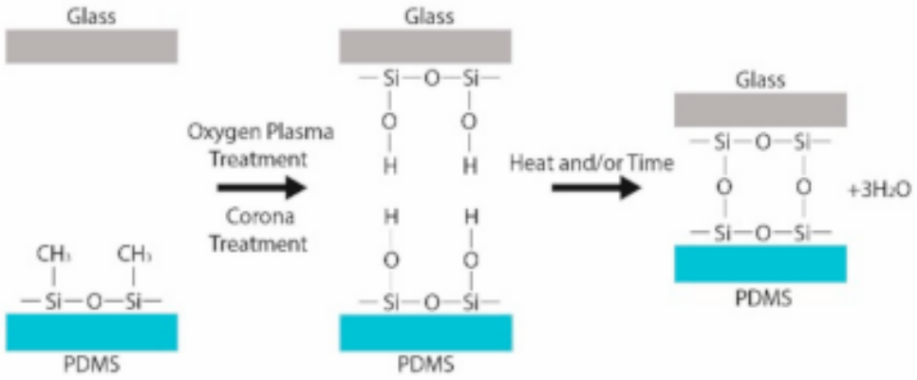

Figure 3.28: Illustration of PDMS surface activation through oxygen plasma treatment. Reproduced by [22].

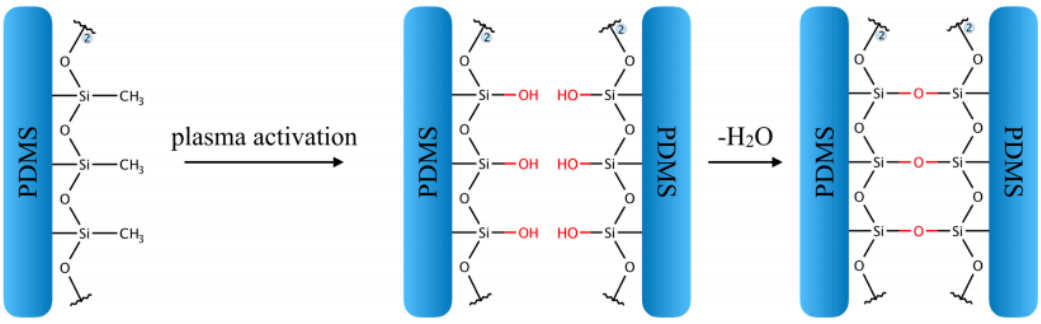

Figure 3.29: Illustration of PDMS surface activation through oxygen plasma treatment. Reproduced by [24].

3.2.8 PEDOT:PSS deposition

A Clevios^{TM} S V4 PEDOT:PSS dispersion in glycols, which is a commercial formulation for screen-printing applications, was used for the OECT channels. The deposition of PEDOT:PSS channel in-between the source and drain electrodes was first tested using a Voltera V-One PCB Printer (Fig. 3.30), which allows to insert in its dispenser a cartridge containing the desired ink, in this case the mentioned PEDOT:PSS S V4 dispersion.

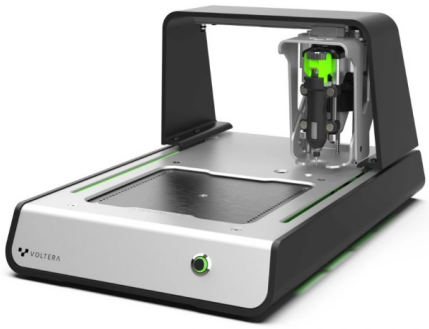

Figure 3.30: Voltera V-One PCB Printer

The dispenser (Fig. 3.31) comprises a plunger that is inserted in the cartridge to extrude the ink. The plunger is driven by a rotating gear mechanism. A nozzle with a diameter of 225 μm is attached to the tip of the cartridge. The Voltera V-One

Figure 3.31: Voltera V-One dispenser

software allows one to change some printing parameters in order to improve the print quality based on the ink properties.
Among all, the two main parameters that were modified were the print height, which is a measure of the distance between the substrate and the nozzle tip, and the ink pressure, which is the amount of force that is exerted on the ink while dispensing.
The results obtained with the Voltera V-One were not satisfying, even after trying with different values of the printing parameters, since the extrusion of ink from the dispenser was not homogeneous.

As a consequence, drop-casting (Fig. 3.32) was instead adopted as deposition technique. This requires to cast some drops of PEDOT:PSS on the substrate. Once that water and solvents evaporate, a PEDOT:PSS channel is deposited.
The main advantages of drop-casting are the ease of implementation, low-cost, and versatility.
On the other hand, the drawbacks of this technique are the lack of control of the uniformity and thickness of the film, and the low reproducibility of the process.
Nevertheless, the results obtained were acceptable for a first attempt of device fabrication. A more reliable deposition process is preferable for the final version of the device.

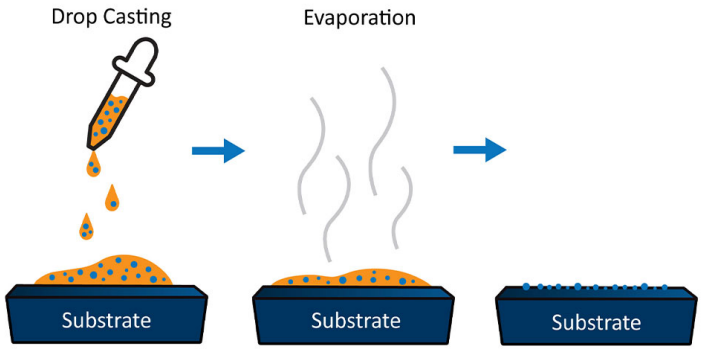

Figure 3.32: Illustration of drop-casting deposition technique. Reproduced by [25].

3.2.9 Electrical connections: formation and passivation

The formation of the electrical connections between the gold electrodes of the device and the ribbon cable was performed using RS PRO conductive silver paint [26]. The choice of using a silver paste to create the contacts was due to the difficulties encountered when trying to solder the device electrodes to the cable. The gold electrodes were in fact damaged, therefore a less detrimental process was needed. Moreover, silver paste has high electrical conductivity and is easily adhered to the Kapton substrate.
To form the contacts, the adhesive paint is first deposited on the gold pads; the ways of the ribbon cable are then stripped to expose the metallic strands. These are twisted in order to facilitate their handling and laid on the gold pads. Finally, silver paint is added to effectively consolidate the contact formation. The process of silver paste deposition and alignment of the gold pads to the cable ways is facilitated by a PDMS guide structure. Once deposited, the paint is left at rest overnight for it to dry.
When the contacts are formed, a passivation step is required. This is crucial to prevent the corrosion and oxidation of the metallic contacts when exposed to the environment and to guarantee a long-term functionality of the device. Furthermore, the electrical insulation protects the device from the formation of alternative conductive paths and reduces the risk of shorting and the onset of electrical noise. Passivation is performed

using an RS epoxy resin compound [27]. This is a two-part resin that is deposited on the electrical connections and is left hardening.

3.2.10 3D printing

3D printing is performed using a Stratasys J35^{TM} Pro 3D Printer (Fig. 3.33).

Figure 3.33: Stratasys J35^{TM} Pro 3D Printer

The printer implements a multi-material jetting photopolymer technology [28].
The photopolymers are jetted on the build platform layer by layer. Each layer is cured with a UV lamp that helps the layers to bond.
The printer allows the design of complex geometries and intricate details; moreover, it is possible to choose between a large range of materials, including biocompatible materials. In this work, 3D printing is used to fabricate the molds for replica molding and to create supporting structures for the device fabrication.
In both cases, the printing process is the following:

- First, a CAD model of the object that has to be printed is prepared; in this work the software used for the CAD designs is Rhinoceros$^{®}$ 8.
- The CAD model is then loaded onto the 3D printer embedded software, GrabCAD^{TM} Print. The software checks if there are any issues in the CAD model and has a tool that fixes potential design errors.
- Moreover, the software allows to set the print settings as preferred. It is important to set the print type as *glossy* when fabricating the molds for replica

molding, otherwise issues in the detachment of PDMS may arise. Also the print resin can be chosen; in this work VeroUltra^{TM} White was utilised.

- The print is then started and when the object is finished it is carefully moved from the building plate with a spatula.
- Afterwards, the support material is manually removed with a spatula. A toothpick is used to remove the materials from the narrower features.
- An ultrasonic cleaning step is performed in isopropyl alcohol (59 kHz for 5 minutes) to remove the support material residuals left.
- The printed object is baked overnight at 110 C°. This step is particularly important for molds, since it allows to fully cure the resin and deactivate the resin photo-initiators, which may compromise the quality of the replication.
- Right after the bake step, the mold is put in an ultrasonic bath in acetone for five minutes at 59 kHz.
- Finally, the mold is dried in the oven at 70 C° for few minutes.

Once dried the 3D printed object is ready to be used.

3.3 OECT electrical characterisation

The OECTs were characterised using an Ossila dual channel source measure unit (SMU) (Fig. 3.34). One channel was connected to the gate electrode to modulate the gate voltage, while the other channel was used to bias the drain electrode. In both cases the ground reference was the source electrode.

Figure 3.34: Ossila SMU used to characterise the OECTs.

The device was mounted on the multi-well plate, then a phosphate-buffered saline (PBS) solution was used as electrolyte. 1.5 milliliters of PBS were inserted inside the

wells, where the Bottom OECTs are placed, while 1 milliliter was deposited within each well insert, where the Top OECTs are located.
The transfer characteristic of the OECTs was obtained by measuring the drain current I_{DS} while sweeping the gate voltage V_G from an initial value to a final one with a voltage increment of 0.01 V. The drain-source voltage V_{DS} was kept costant at -0.6 V. The sampling rate was set at 4096. Different repetitions of the curve were measured.
The OECT transfer characteristic allows to verify the correct behaviour of the transistor. By inspecting the curve it is possible to notice if the device turns off within an acceptable voltage range and check if the values of the currents involved are consistent.
The main figures of merit that can be obtained from the transfer characteristic are the I_{ON}/I_{OFF} ratio and the transconductance g_m.
The first parameter corresponds to the ratio between the device current when the OECT is turned on and the current flowing when the device is turned off. An higher value of the I_{ON}/I_{OFF} ratio is preferrable in biosensing applications to have a better signal-to-noise ratio and thus a lower limit of detection [2]. Moreover, a lower Off current causes a lower power consumption of the device.
The OECT transconductance is obtained by deriving the drain current with respect to the gate voltage $\left(g_m = \frac{\partial I_{DS}}{\partial V_G}\right)$. It is an important parameter as it is linked to the ability of the device of amplifying an input signal. A higher transconductance corresponds to a higher sensitivity of the transistor, since a lower variation of the gate voltage V_G is necessary to produce the same change in the output current I_{DS}.

3.4 Caco-2 cells membrane analysis

The biosensing platform's ability of analysing the barrier integrity of a cellular membrane was tested using a Caco-2 cell culture. The various steps involved in the creation of the cell culture and the subsequent analysis were carried out by BrainDTech company.

The culture medium composition is the following:

- DMEM High Glucose with L-Glutamine
- 20 % FBS
- 1 % NEAA
- Penicillin-Streptomycin

The Caco-2 cells are first cultured in a T25 flask with 5 ml of culture medium. The medium is replaced every 2 or 3 days. Once a confluence of about 90% $\div$ 95% is reached, cells are counted with a hemocytometer.
Afterwards, cells are ready to be seeded in the transwell inserts.
The device is first sterilised in an autoclave (121 C°, 20 mins.). Bottom OECTs

are then integrated in the wells, fixed with the aid of a small piece of Kapton tape. Transwell inserts are placed inside the wells and Top OECTs are integrated inside them, always fixed with some Kapton tape (Figs. 3.35 and 3.36).
About 150000 cells are then seeded within each transwell insert. 1 *ml* of medium is inserted in the inserts (apical side) and 1 *ml* in the well compartments (basolateral side) (Fig. 3.37 [29]). The medium is changed every two days. The whole setup is finally placed in the incubator.

Figure 3.35: Whole setup after sterilisation, before Caco-2 cells are seeded.

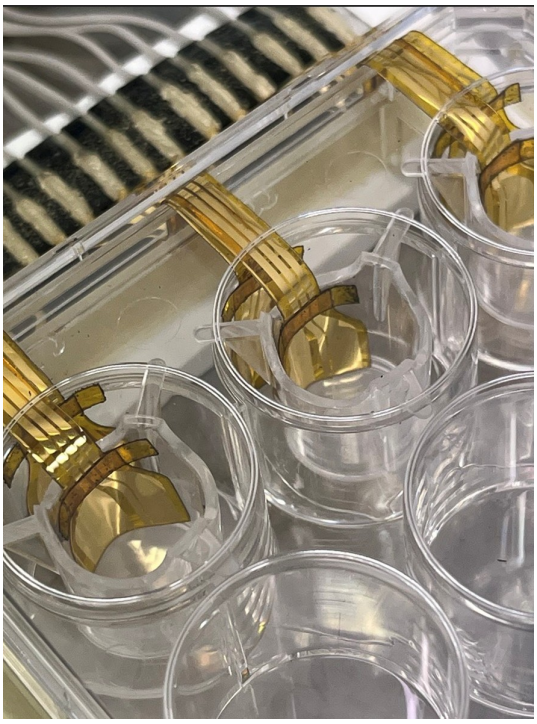

Figure 3.36: Close-up view of the Top and Bottom OECTs integrated in the multiwell plate.

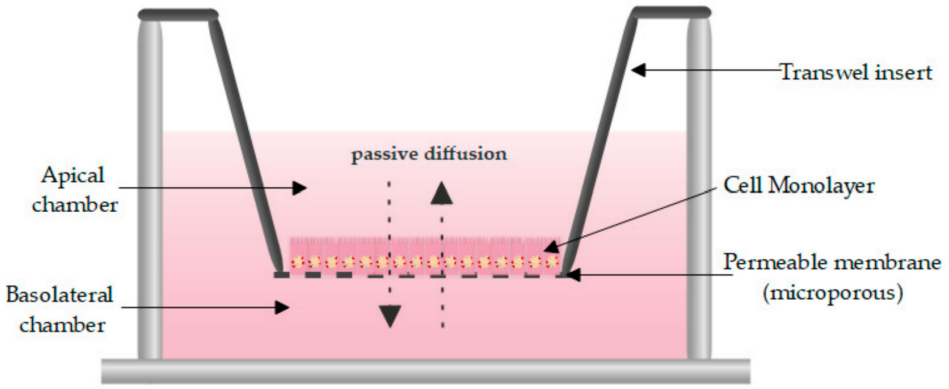

Figure 3.37: Illustration of the setup once Caco-2 cells are seeded in the transwells, with culture medium inserted in both the apical and basolateral compartments. Reproduced by [29].

Once the cells are seeded, they begin to form junctions and unite in a membrane. During this time, the membrane TEER is continuously monitored to assess the barrier integrity.
This is done using the device in the amperometric configuration. In particular, a square wave is periodically applied between the Bottom and Top gate electrodes of each well and the resulting current is analysed. The gate electrodes are chosen because they are the larger ones. The current is caused by the movement of the electrolyte's ions across the membrane, going from the apical to the basolateral compartment or vice versa. The signal applied between the two electrodes is the following:

- 0.5 V for a time interval $t_{on} = 50\ ms$
- -0.5 V for a time interval $t_{off} = 50\ ms$
- 0 V for a time interval $t_{sleep} = 2\ mins$

A negative and opposite voltage is applied in order to avoid accumulation of charge. Continuous monitoring is performed for seven days. The current values are acquired during t_{on} and t_{off} with a sampling time of 2.5 ms and a resolution of 780 nA. Therefore, the transient response of the current to the application of a square wave is obtained and is used to analyse the barrier integrity.

Chapter 4

Results

4.1 Device fabrication

4.1.1 Gold electrodes

The initial step in the device fabrication is the creation of the gold electrodes through a traditional subtractive lithographic process. All processes presented below were performed in the PiQuET cleanroom facility at the Istituto Nazionale di Ricerca Metrologica in Turin by authorized operators.
The main process steps involved in the fabrication of the gold electrodes are the following:

- First, gold is evaporated on a 25 μm thick Kapton sheet.
- AZ 1518, a positive photoresist, is spin-coated on the gold-coated Kapton sheet.
- Afterwards, a soft-bake step is necessary, therefore the Kapton substrate is put on a hot plate at 110 C° for one minute.
- The following step is the UV-exposure of the resist. A CAD version of the electrodes' geometry is uploaded on the Microtech Laser Writer LW405A and is used as a mask for the exposure.
- Once the resist is exposed it needs to be developed. This allows the exposed portions of the resist to be removed, keeping only the non-exposed parts. To do so, the Kapton sheet is immersed in a solution of water and AZ 400K developer with a 3:1 volumetric ratio for 40 seconds.
- Then, the exposed gold is wet etched using Au etcher for few seconds. The undeveloped photoresist prevents the gold underneath from being etched, allowing to have the desired gold electrodes layout.
- Finally, the remaining undeveloped photoresist is removed with a mixture of acetone and isopropanol.

A schematic illustration of the subtractive lithographic process performed is shown in Fig. 4.1. The final result of the gold electrodes is shown in Fig.4.2 and in Fig.4.3 for the alternative device design.

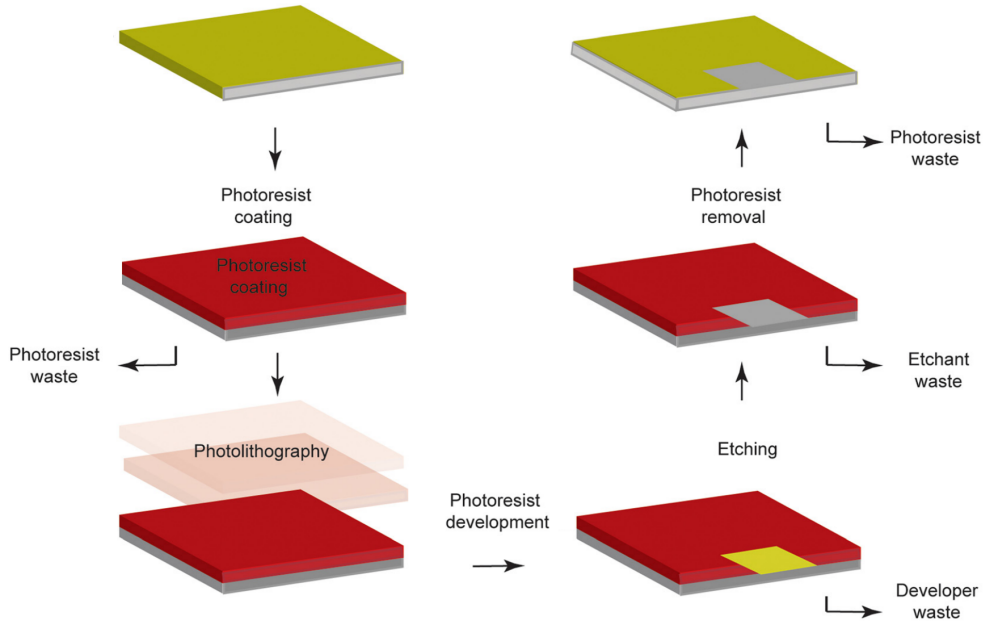

Figure 4.1: Schematic of the lithographic process steps used in gold tracks fabrication. Adapted by [30].

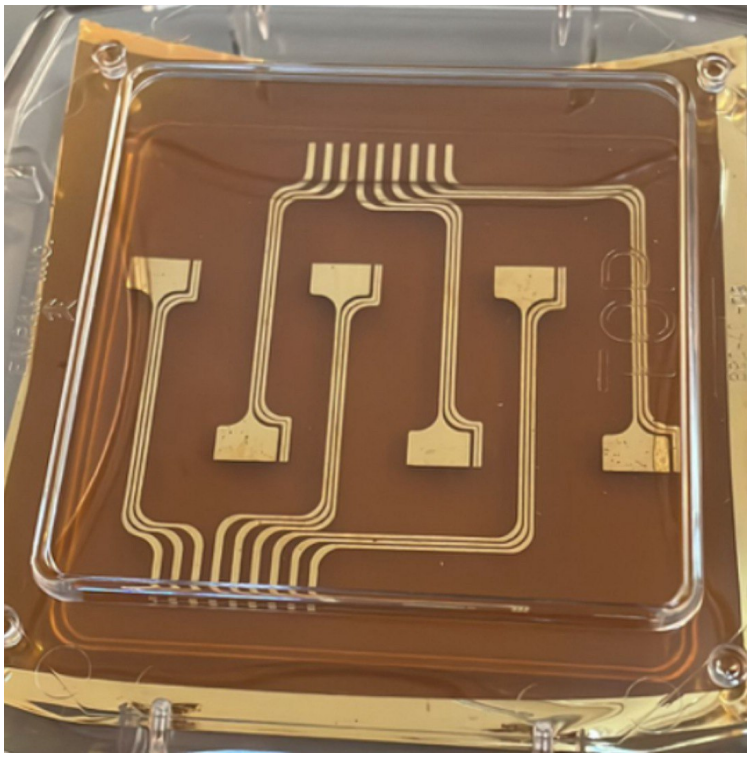

Figure 4.2: Gold electrodes on Kapton sheet obtained through the described lithographic processes.

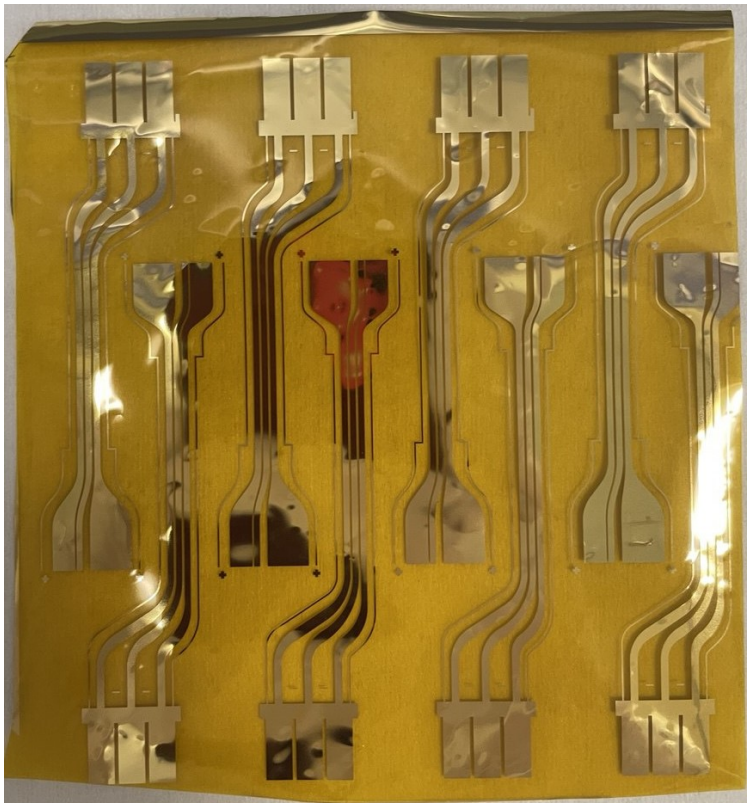

Figure 4.3: Gold electrodes on Kapton sheet - alternative device design.

4.1.2 PDMS spin coating

Once the gold electrodes are patterned on the Kapton substrate, the subsequent step in the device fabrication is the deposition of a thin layer of PDMS on it. This is done through spin-coating (Fig. 3.23).
For both the Top and Bottom structures, the Kapton sheet is fixed to a four-inch silicon wafer with some Kapton tape. The PDMS is first spun on the back side of the two structures, i.e. the side in which the gold electrodes are not present.
In order to spin-coat PDMS it is first necessary to secure the silicon wafer on the spin-coater's vacuum chuck. Then some PDMS is poured on the Kapton substrate. Finally, the process parameters are set as desired and PDMS is spun.
The process recipe is composed of two phases. The first phase is used to spread the poured PDMS uniformly across the substrate, while the second phase allows the PDMS layer to reach the correct thickness based on the chosen spinning settings.

The parameters used for the PDMS deposition were the following:

PDMS spreading phase (1^{st} phase)

- Spinning acceleration: 500 rpm/s
- Spinning speed: 500 rpm
- Spinning time: 5 sec

PDMS thinning (2^{nd} phase)

- Spinning acceleration: 500 rpm/s
- Spinning speed: 3000 rpm
- Spinning time: 30 sec

Once the PDMS is successfully spun, the devices are put in a Memmert lab oven in order for the PDMS to cure. The PDMS was left for about an hour at a temperature of 100 C°.
Afterwards, PDMS is again spun on the top side - the one where gold electrodes are present - of the two structures. The spin-coating process parameters are the same as previously used. The spin-coating process is again followed by a bake to cure the PDMS.

Spinning PDMS on the two structures that compose the device has two main purposes.
First, PDMS allows to passivate the gold electrodes so that they do not get damaged or corroded upon exposure to the environment. Secondly, the two PDMS layers allow to bond the Top and Bottom structures one to the other. Indeed, PDMS-to-PDMS bonding reaches good adhesion strength and is suitable for attaching the two structures.

An analysis of the different PDMS thickness values obtained by varying the spinning speed was performed through profilometry. The same Kapton sheet used for the device was adopted as substrate for the analysed samples and fixed with Kapton tape on a 2-inch wafer. PDMS was then poured and spun. The analyses were performed maintaining the spinning time constant at 30 seconds and varying the spinning speed. The different PDMS layers were then analysed with the Tencor P-17 profilometer and the different thickness values were collected.
Some examples of the profiles obtained are presented in Figs. 4.4 and 4.5.

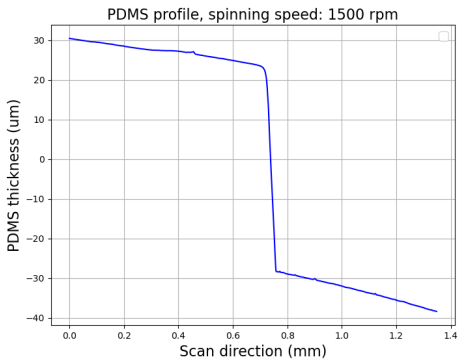

Figure 4.4: Graph showing the step height of a PDMS layer deposited with spin coating at 1500 rpm for 30 seconds.

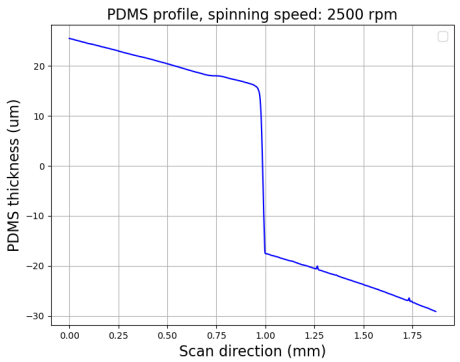

Figure 4.5: Graph showing the step height of a PDMS layer deposited with spin coating at 2500 rpm for 30 seconds.

The results obtained after collecting the various thickness values are shown in figure 4.6. PDMS thickness was measured respectively for the following spin speeds expressed in rpm: 500, 750, 1000, 1500, 2000, 2500, 3000, 3500, and 4000. The spin time was instead kept constant at 30 seconds.

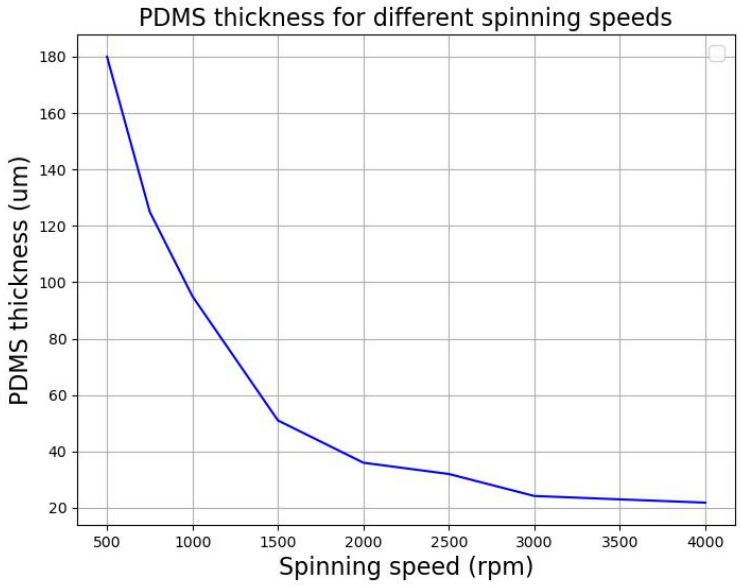

Figure 4.6: Graph showing how PDMS thickness varies with different spinning speeds.

The trend of the resulting curve is the expected one. Indeed, by increasing the spinning speed one would expect the PDMS film to become thinner due to the higher centrifugal spreading, and this is confirmed in the graph of Fig. 4.6. The analysis is also coherent with an analogous analysis found in the literature, shown in Fig. 4.7 [31].

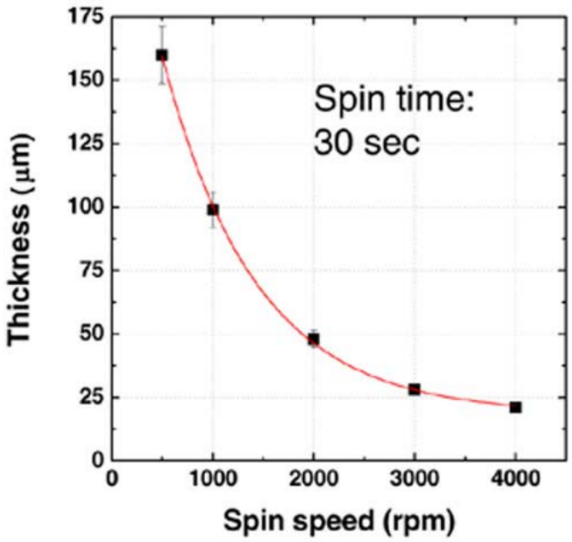

Figure 4.7: Graph showing the behaviour of spin-coated PDMS layers thickness vs spin speed. Spin time fixed at 30 sec. Reproduced by [31].

The comparison of the two graphs shows good consistency, considering also the differences in the two experimental setups in terms of substrate used and wafer dimension.

4.1.3 Laser cut

When PDMS is spun on both sides of the devices, the Top and Bottom structures are cut from the substrate using a Microla Laser Slider. Before cutting the device, a CAD file with the incision geometry has to be uploaded on the embedded instrument computer.
Afterwards, to correctly perform the cut, the focal distance between the laser spot and the substrate has to be adjusted. This is done through the specific button of the laser marker that automatically focuses the laser. An adequate focusing is critical to obtain an accurate and clean cut.
Next, a precise alignment of the substrate on the instrument work table is necessary, since the laser has to precisely run along the gold tracks present on the Kapton sheet. The alignment is facilitated by the specific feature of the laser instrument that shows the pattern of the laser spot across the substrate. Moreover, in case of small adjustments, the embedded software allows to geometrically translate and rotate with high precision the virtual position of the cut geometry on the work table, so that it is not necessary to manually move the substrate. Additionally, the incision geometry is designed to have a 1 mm offset with respect to the gold electrodes, to have some margin of operation and to account for the laser slider uncertainty.
Finally, once the alignment is completed, the laser parameters of the cut process recipe need to be carefully chosen for the specific needs.

The laser parameters used for the device are reported below:

- **Power**: 17 %
- **Scan speed**: 50 mm/s
- **Frequency**: 1.5 kHz
- **Repetitions**: 2

These values used in the cutting process were selected after an empirical analysis was conducted on some testing Kapton sheet samples on which PDMS was spinned. The purpose of the analysis was to find the correct parameters in order to obtain a precise cut and minimize the unwanted side effect of graphene formation on the contour of the device due to the burning of the Kapton substrate. After several tests, the optimal laser parameters delivering the better results were the ones reported above.

The results of the cutting process are presented in Figs. 4.8 and 4.9.

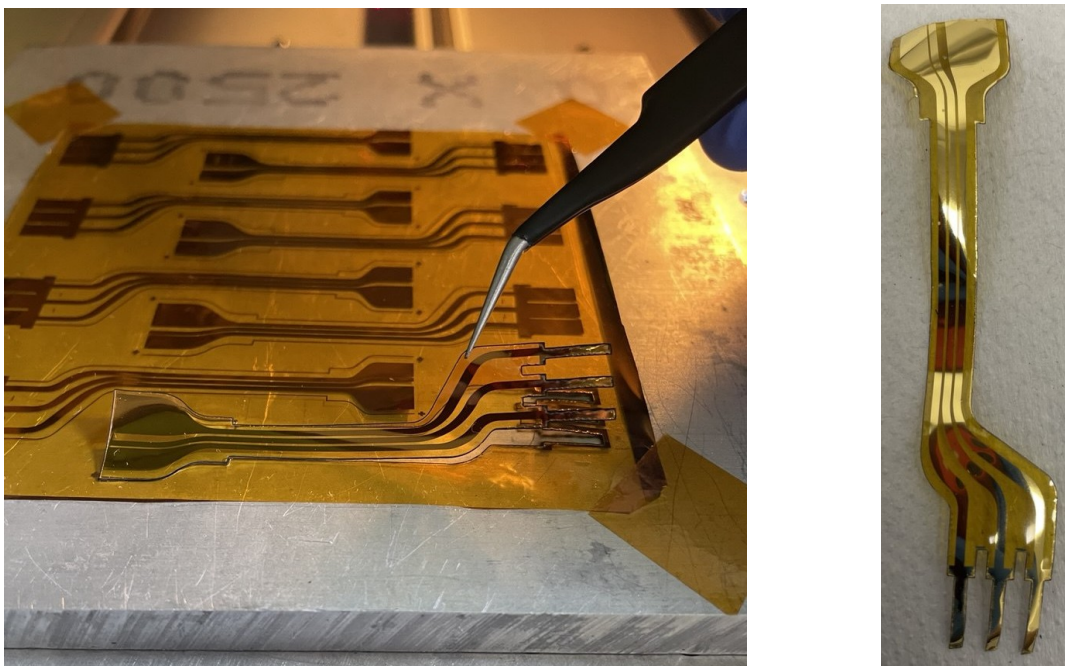

Figure 4.8: On the left, the Kapton sheet with the alternative design geometry mounted on the laser slider work plate after the cut has been performed. On the right, the alternative design Bottom structure after the laser cut.

Figure 4.9: Standard design Top and Bottom structures after the laser cut.

4.1.4 Plasma bonding

Plasma bonding is only needed for the standard design device, since the Top and Bottom structures need to be attached. The alternative design does not require a bonding step.
Before bonding the Top and Bottom structures, PDMS needs to be removed from the terminal parts of the gold tracks, the ones that will be immersed in the electrolyte solutions in the wells. This is done by carefully incising the edge of the section of PDMS that has to be removed with a laboratory scalpel. Afterward, PDMS is gently stripped away with a toothpick. The previous steps need maximum attention, since it is important not to damage the gold electrodes.
Once the two structures are prepared, they are arranged on a metal slab. The back side of the Top structure and the top side of the Bottom structure are placed face up, since they need to be exposed to the oxygen plasma for the surface to be activated and then bonded. The oxygen plasma treatment is performed using a Diener Atto plasma system. Once the two structures are placed in the plasma chamber, the already present "PDMS activation" process recipe is performed:

- First, a vacuum is created in the chamber;
- then, oxygen is introduced until a pressure of 0.7 *mbar* is reached;
- finally, the oxygen plasma is activated for 30 seconds.

At the end of the plasma treatment, the structures are removed from the chamber and a 3D-printed cover structure is placed on the Top structure in order to cover the terminal half portion of the branches, which is not intended to be bonded to the Bottom structure. Indeed, the final parts of the branches of the two structures need to be separated, since they are supposed to be split when mounted on the multiwell plate - the Bottom structure branches will enter the wells, while the Top structure branches are placed inside the well inserts -.
Once the cover structure is placed, the Bottom structure is put on top of the Top one with a pair of tweezers, making sure to contact the two sides whose surface

was activated. The two structures are precisely aligned and then pressed together to obtain a good bonding of the portions between which the cover structure is not interposed.
After manually pressing for about a minute the two structures, they are put in an oven at 75 C° for 10 minutes to increase the bonding strength.

4.1.5 PEDOT:PSS channel deposition

As mentioned, a preliminary version of the device is fabricated by manually depositing PEDOT:PSS on the OECT channels. This method is only adopted for a first tentative attempt; more reliable techniques are necessary for the final version of the device.

The channel organic polymer is deposited through manual drop-casting from a Voltera V-One dispenser which mounted a PEDOT:PSS dipersion cartridge. A 225 μm nozzle was used. Drops of the PEDOT:PSS dispersion were deposited between the source and drain electrodes to form the OECT channel. An estimated volume of 6 μl of PEDOT:PSS dispersion was cast.
The devices were then put in an oven at 110 C° for 30 minutes, in order for the residual water and solvents to evaporate and to improve the film conductivity.
The final film thickness was not measured with a profilometer to avoid ruining the channel, but analogous experiments performed with a similar setup in the same laboratory showed a PEDOT:PSS thickness of about 1.5 $\div$ 2 μm. Therefore, this can be considered a good estimate for the final thickness.

Figs. 4.10 and 4.11 show an example of an OECT once the channel was deposited.

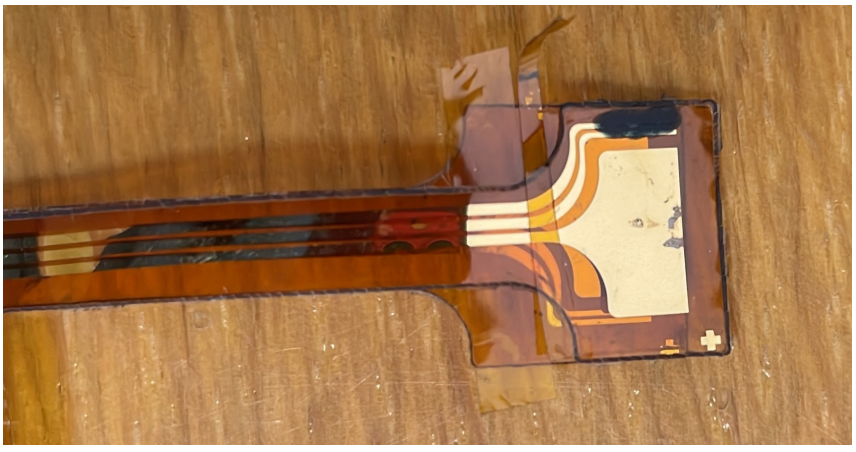

Figure 4.10: PEDOT:PSS channel deposited through drop-casting.

Figure 4.11: OECT mounted on the multiwell plate once the PEDOT:PSS channel is deposited.

4.1.6 Contact formation with conductive silver paste

At the end of the bonding process, the device comprising the Top and Bottom OECTs is completed. The next step in the fabrication is the formation of the electrical contacts that will connect the device with the flat cable and the D-Sub connectors. The contacts are made using the RS PRO conductive silver paint.
Before creating the contacts it is important to make sure that PDMS is not present on the gold pads of the device. If this is not the case, the PDMS can be removed using a laboratory scalpel and a toothpick as previously described.
Afterwards, the flat cable wires are stripped in order to expose the stranded conductors that are going to be connected to the device electrical pads. The electrical strands are then twisted to favour the contact formation.
Moreover, to facilitate the deposition of the silver paint, a PDMS supporting structure was fabricated. The purpose of the structure is to avoid the formation of short-circuits, since the different sections of the supporting structure separate the device contact pads and prevent the deposition of some silver paste across two adjacent contacts. Furthermore, the PDMS structure also lends mechanical stability to the contact region, which is subjected to mechanical stress. The CAD version of the supporting structure is shown in Figs. 4.12 and 4.13.

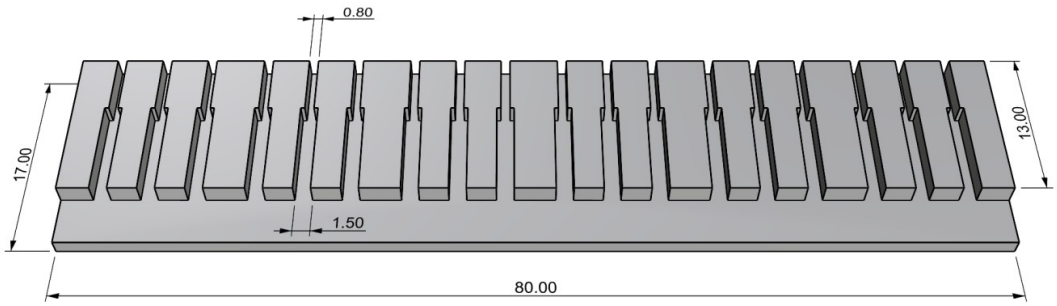

Figure 4.12: CAD version of the PDMS guide structure used to facilitate the contact formation. The reported measures are expressed in *mm*.

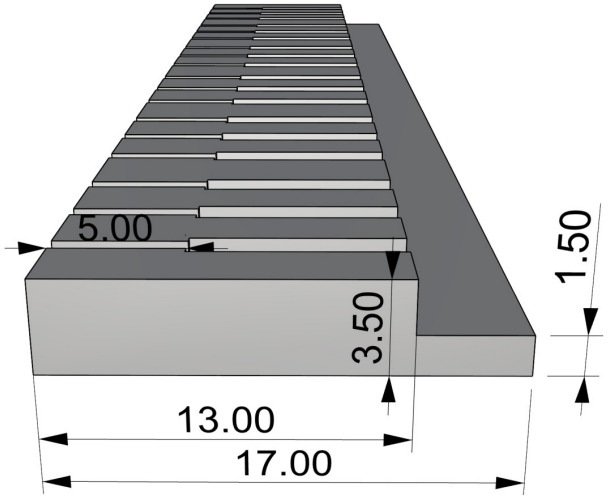

Figure 4.13: Lateral view of the CAD version of the PDMS guide structure used to facilitate the contact formation. The reported measures are expressed in *mm*.

Each channel-like section of the PDMS guide structure is supposed to host a different electrical contact, and the sections are separated by barriers to avoid creating short-circuits when depositing the silver paint. Each channel is composed of a narrow region and a wider one (Fig. 4.14). The narrower parts house the non-stripped part of the flat cable's ways, and they are made narrow enough so that the wire's insulating sheath can fit perfectly and remain fixed. The wider portions instead are the ones where the device gold electrodes are accommodated together with the metallic strands of the cable ways. Finally, the portion of the structure without barriers endows the device with mechanical stability.

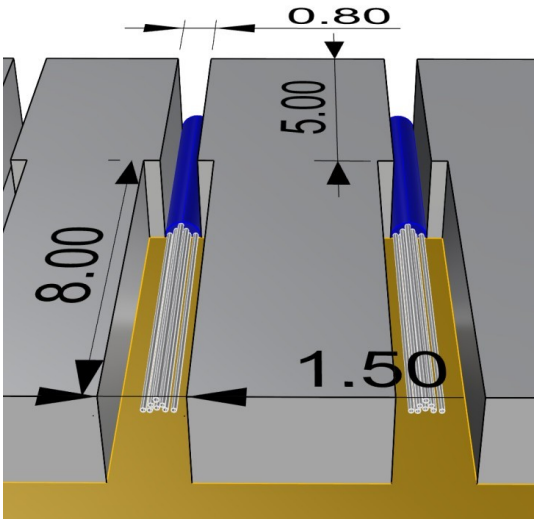

Figure 4.14: Close-up view of the PDMS guide structure. The narrower section of the channel houses the non-stripped part of each cable way, represented in blue, thus fixing it to the PDMS guide. The wider section is where the device gold electrodes (in yellow) are placed, with the metallic strands of the stripped way above, represented by the grey wires. All measures are expressed in *mm*.

The formation of the contacts involves the following steps:

- First, the device is placed with the gold electrodes allocated in the designated parts of the supporting structure (Fig. 4.15);
- then, silver paint is deposited directly on gold with a toothpick, in-between each barrier;
- each stripped wire of the flat cable is then fixed to the narrower part of the PDMS structure channels. The fixing is favoured by the fact that the non-stripped parts of the wires, still having the insulating sheath around, fit perfectly inside the narrow channels, thus firmly blocking the wires to the supporting structure;
- the twisted stranded conductors of the stripped wires are pushed with a toothpick towards the gold electrodes, so that they are well immersed in the previously deposited silver paint;
- once the conductors are attached to the electrodes, an additional deposition of silver paint is performed to completely fill the cavity where the gold electrodes are placed, thus ensuring a good contact formation (Fig. 4.16);
- finally, the silver paint is left to dry overnight.

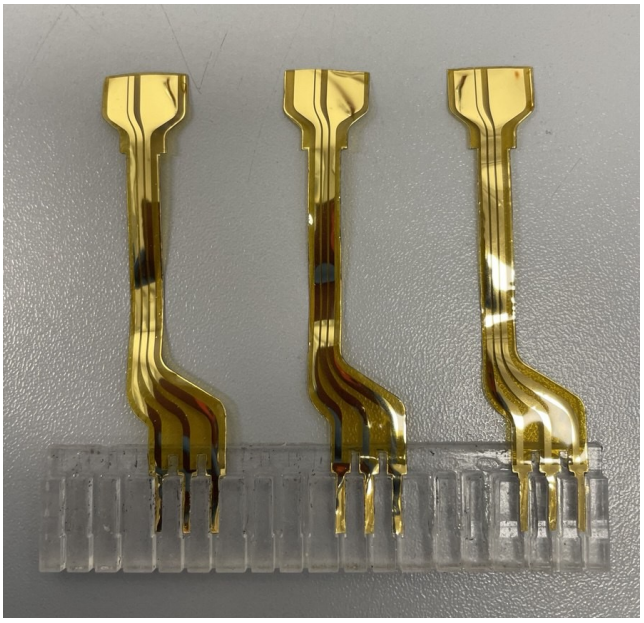

Figure 4.15: Gold electrodes positioned on the PDMS guide.

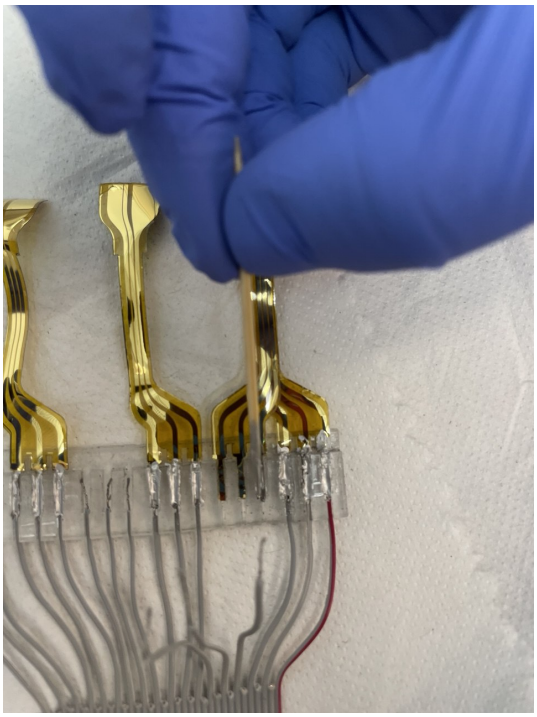

Figure 4.16: Silver paste is deposited with a toothpick to form the contacts.

When the paint has dried, the device appears as in Fig. 4.17.

Figure 4.17: Final result of the device once the contacts with the ribbon cable are formed.

The quality of the contacts is verified with a multimeter, to ensure that the electrical connection from the flat cable up to the terminal parts of the gold electrodes, that are going to be in contact with the electrolyte, is uninterrupted.

4.1.6.1 Contact passivation

Once the electrical connections have formed they need to be passivated.
To passivate the contacts, RS 199-1468 epoxy resin is used, a two-part resin that protects electrical components from chemicals and water even in harsh conditions. When cured, the resin hardens and becomes very tough.
The preparation involves mixing the resin and the hardener in a weight ratio of 1:1. The mixture is then stirred with a laboratory spatula, so that the two components are well mixed.
Afterwards, the mixture is left to rest for about 90 minutes. During this time the air bubbles generated when stirring are removed, and the resin starts hardening, thus becoming more viscous, which is favourable for our purpose. Indeed, the resin does not have to spread too much when poured, since it is supposed to remain on the PDMS guide without spilling out of the edges. Therefore, a harder texture of the resin is preferable.
The resin is deposited on the contacts with a toothpick, covering the whole PDMS supporting structure.
Once deposited, the epoxy is left to harden overnight, with the device kept horizontally to prevent the resin from overflowing. The hardened resin also gives mechanical stability to the device. This is crucial since the handling of the device-cable system was particularly delicate in the area where contacts are formed.

The final result of the device is shown in Fig. 4.18.

Figure 4.18: Image of the device after the contacts are passivated.

A close-up view of the PDMS guide structure with the epoxy resin is depicted in Fig. 4.19.

Figure 4.19: Close-up view of the passivation of the contacts. The resin endows the device with mechanical stability.

4.1.7 Multiwell plate support

When the ribbon cable is successfully connected to the device, the biosensing platform is mounted on the multiwell plate and fixed with some Kapton tape. To favour the handling and transport of the multiwell-device system, a supporting structure is fabricated. A CAD model is realised using Rhinoceros® 8 3D program. The structure is then 3D-printed.

The CAD model is shown in Fig. 4.20; in blue are highlighted the features through which the multiwell plate is wedged to the support, thus remaining fixed.

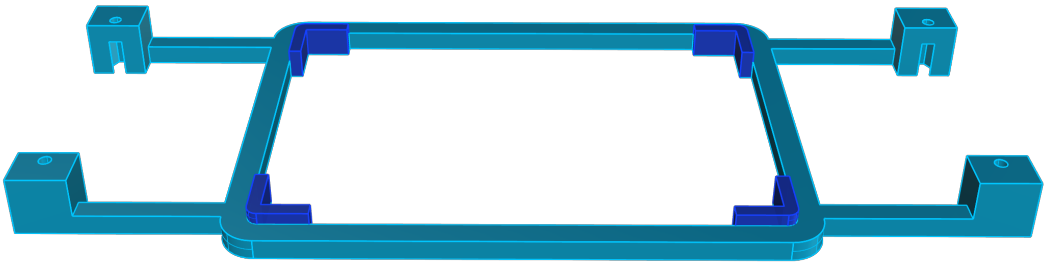

Figure 4.20: CAD version of the support structure. In blue the features used to fix the multiwell plate to the support.

An illustration showing the plate mounted on the support structure is shown in Fig. 4.21.

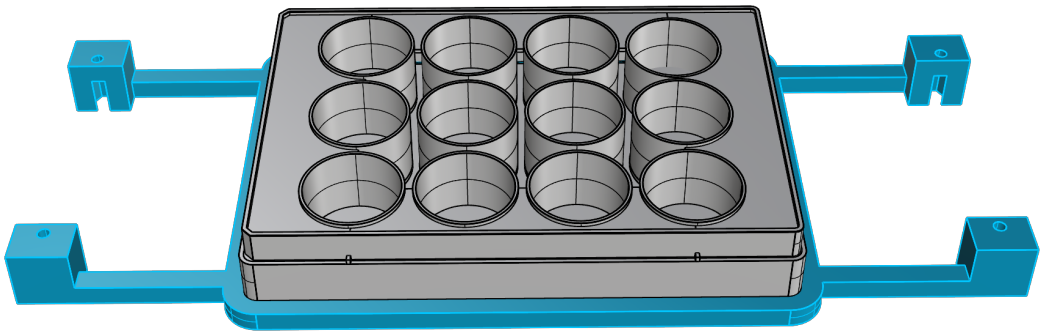

Figure 4.21: CAD illustration of the multiwell plate mounted on the support structure.

The branches protruding from the base of the plate are designed to hold the D-Sub connectors to which the ribbon cables are crimped. In this way, the overall mechanical stability of the system is improved as the stress induced on the contacts between the cables and the devices when the connectors are connected is reduced, since the D-Sub connector is fixed to the structure. Furthermore, the system is easier to transport, especially in and out of the incubator. Concerning the D-Sub connectors, they are fixed to the support structure with two screws. Four holes are created at the end of the branches, two on each side, with a diameter of 3 mm, in order to hold the screws. When the structure is printed, the screw thread is forced in the holes by screwing them inside.
Moreover, a hollow feature (Fig. 4.22) is created aimed at holding the bolt to ease the fixing of the connectors.

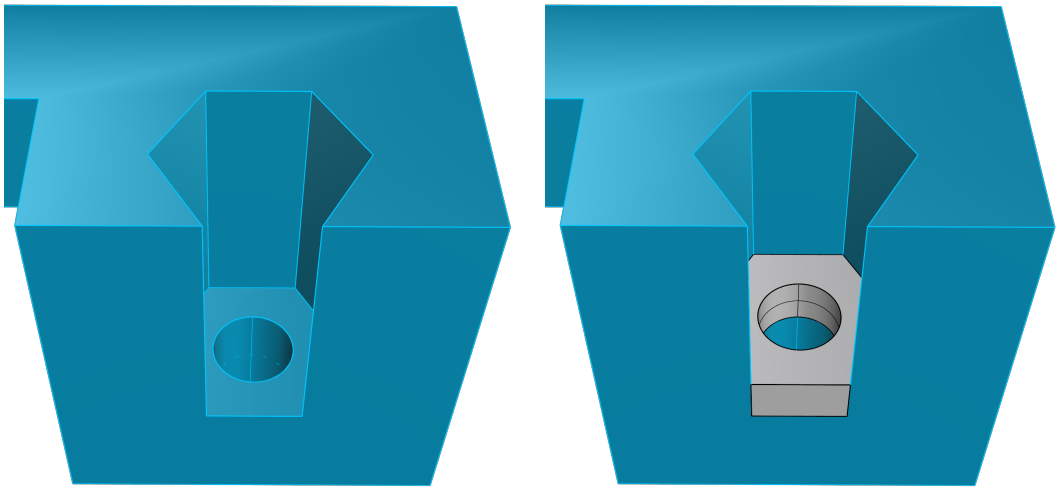

Figure 4.22: On the left, the exagonal cavity designed on the back of the structure's branches to hold the bolt to ease the fixing of the connectors with the screw. On the right, an illustration of the bolt slotted in the cavity.

Once the device is mounted on the structure, the overall system is shown in Fig. 4.23.

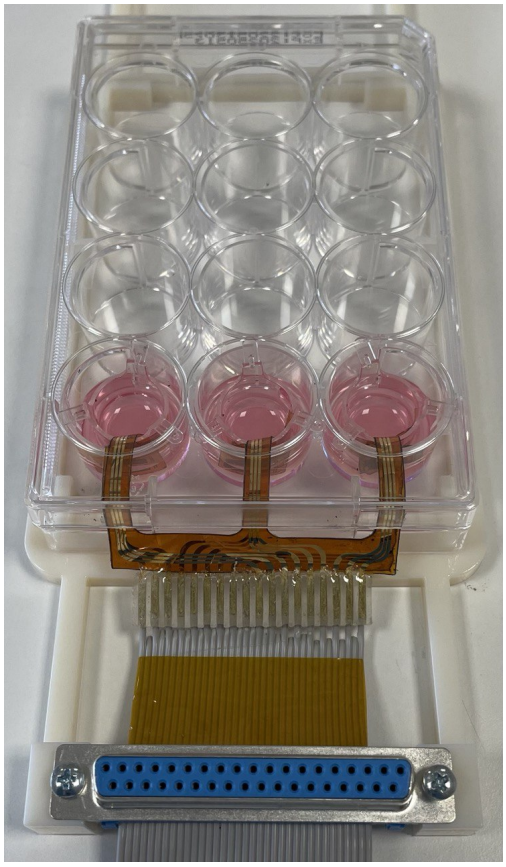

Figure 4.23: View of the device mounted on the supporting structure.

Small variations to the geometry of the supporting structure were adopted for the alternative design device; in particular, the branches were extended in length, in order to leave more space to the ribbon cable ways. The alternative design device, as

mounted on the supporting structure, is shown in Fig. 4.24.

Figure 4.24: View of the alternative design device mounted on the supporting structure. The branches of the structure were made longer to better accommodate the ribbon cable.

4.2 Device biocompatibility

Being involved in the analysis of a cellular membrane, the device biocompatibility has to be tested to ensure that no harmful effects are caused to biological samples.

A first test was conducted using ethanol to sterilise the device. First, the device was electrically characterised, then it was put in a bath with a 70% ethanol solution in water for an hour. Afterwards, the device was washed and its electrical behaviour was then inspected to see if the device was damaged during the sterilisation in ethanol.

Following the positive outcome of the ethanol bath, an autoclave sterilisation was then performed, which is stronger and more effective. The device was put in the autoclave chamber at 121 C° for 20 minutes. After the device was re-characterised to see if the autoclave step had left any consequences, a partial delamination of the PEDOT:PSS channel and of the gold pads of the OECT was observed. Autoclave sterilisation might be the cause of this unwanted effect, but also the PEDOT:PSS deposition process and the high voltages involved in the electrical characterisation might have affected the device integrity.

In order to test the biocompatibility of the device, the device underwent a test to verify the contamination of a cell culture medium. The device was first sterilised in an autoclave and then integrated under a chemical hood on the multi-well, which had been sterilised as well. The system was then left in an incubator with a cell culture medium for four days. The setup is shown in Figs. 4.25 and 4.26.

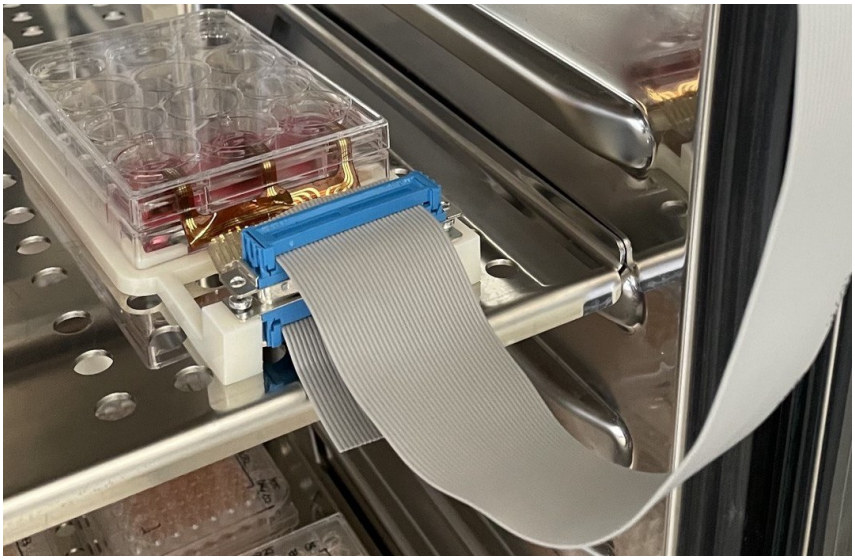

Figure 4.25: System setup placed in the incubator to undergo a test with cell culture medium to verify its biocompatibility.

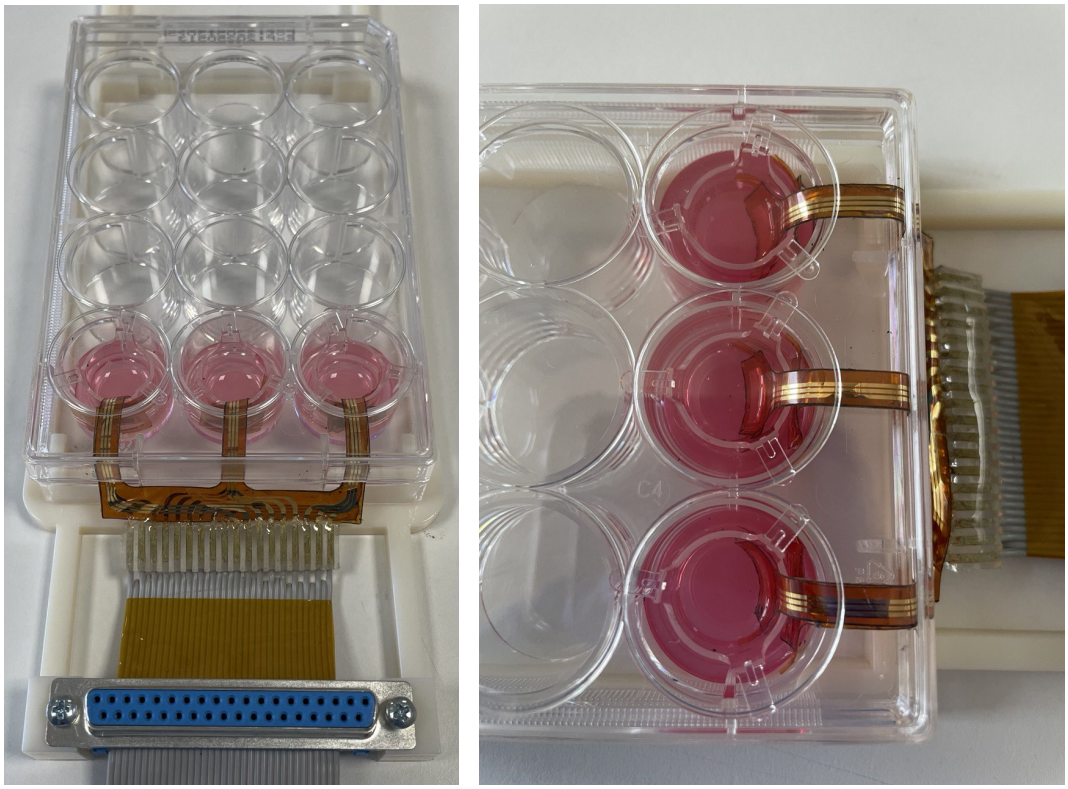

Figure 4.26: Device setup with cell culture medium inserted in the wells and transwell inserts.

After the incubator test no bacterial growth was observed during the third and fourth day, suggesting that the device is biocompatible, as it did not contaminate the biological sample.
PEDOT:PSS was observed to be deliminated, therefore an alternative deposition method has to be utilised and verified, as drop-casting is not reliable.

4.3 OECT electrical characterisation

Considering the many difficulties encountered with respect to the deposition of the PEDOT:PSS on the OECT channel, the following analysis concerning the electrical characterisation of the OECT devices has to be considered as an approximate analysis, whose purpose is just a first general evaluation of the device functionality.

A first device (OECT1) was characterised using the Ossila SMU. The device transfer characteristic was obtained sweeping the gate voltage (V_G) from 0 V to 1 V. The curve obtained is shown in Fig.4.27.

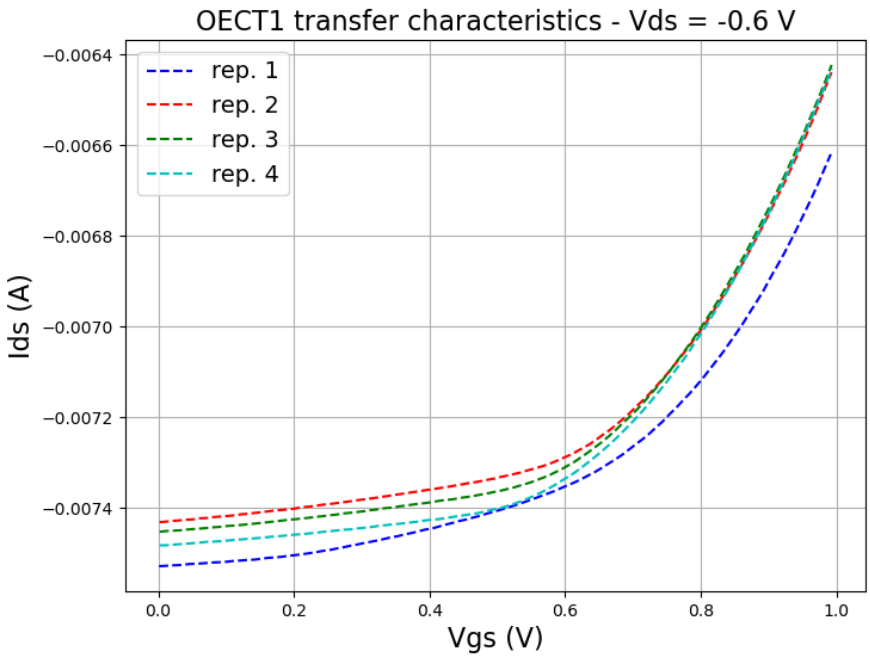

Figure 4.27: OECT1 transfer characteristic.

The device transfer characteristic shows that the OECT does not turn off within the expected voltage range. Despite a slight decrease of the drain current (I_{DS}), the device is still in the ON state when a voltage of 1 V is applied at the gate. The reasons behind this behaviour may be different. The gate area might be too small or the gate capacitance might be too low thus causing a less efficient de-doping of the PEDOT:PSS channel.
Another reason might be the difficulty of ions to penetrate in the channel due to the PEDOT:PSS properties.
Other causes may involve the electrolyte properties or the initial conductivity of the channel, which might have been too high.

A second OECT (OECT2) was characterised using a larger voltage sweep, reaching a gate voltage V_G of 1.8 V. The resulting transfer characteristic (Fig. 4.28) shows

that the device turns off.

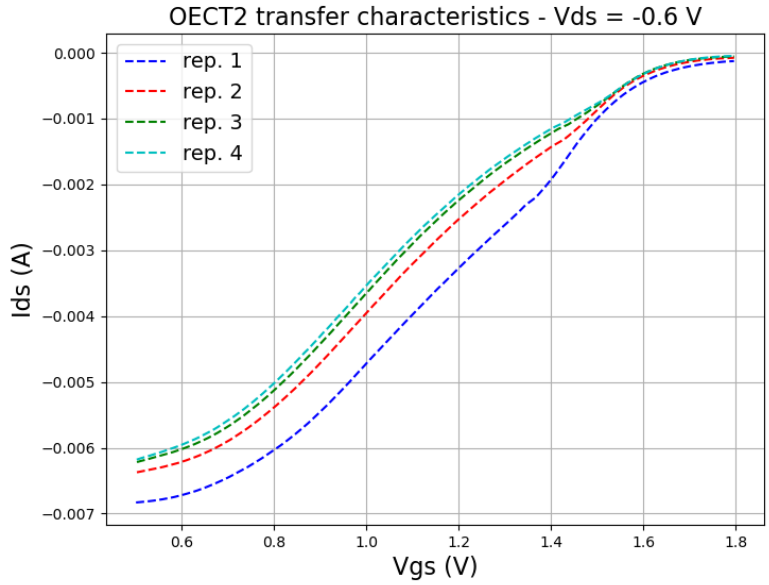

Figure 4.28: OECT2 transfer characteristic.

The drain current I_{DS} in the On state is of the order of a few milliamperes as expected, while the I_{on}/I_{off} ratio is of the order of 10^2, which is acceptable.

Both the devices were then sterilised in ethanol (bath in a 70% ethanol water solution) and their transfer characteristic was measured afterward (Figs. 4.29, 4.30).

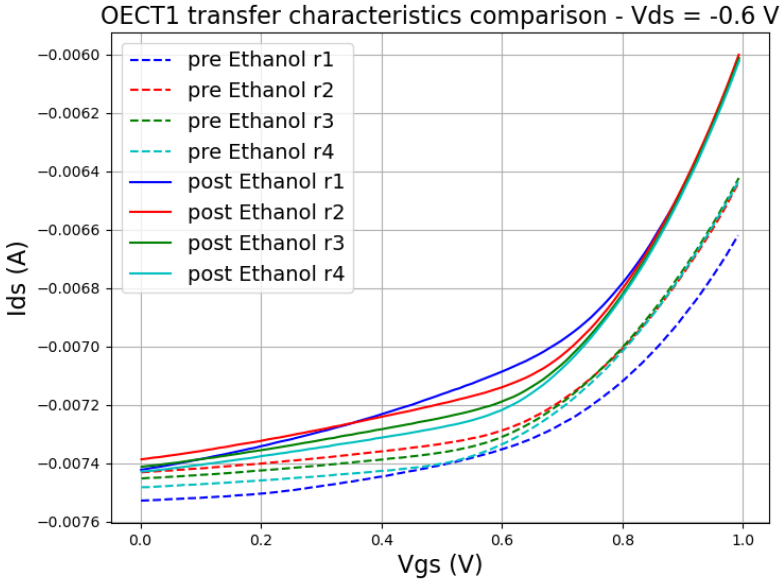

Figure 4.29: OECT1 transfer characteristic comparison before and after the ethanol sterilisation.

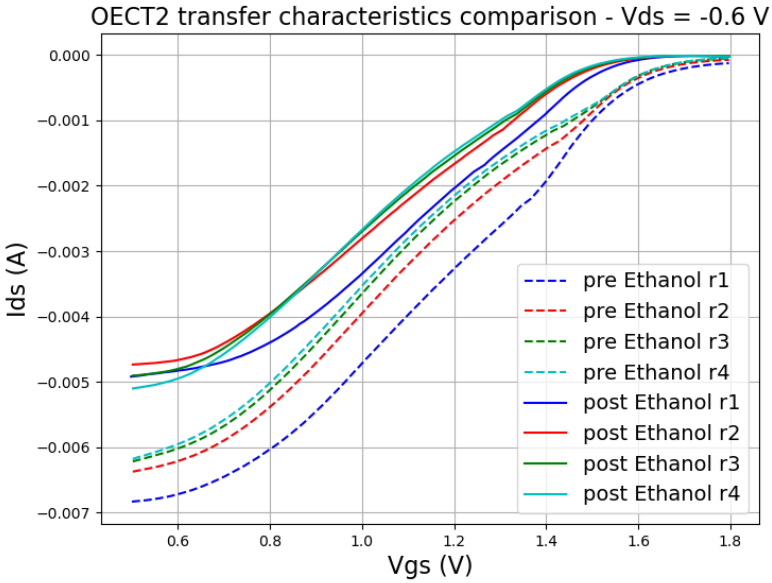

Figure 4.30: OECT2 transfer characteristic comparison before and after the ethanol sterilisation.

Overall the ethanol sterilisation reduces the currents of the devices, but the trend is maintained, so the device operation does not seem to be affected by the sterilisation process. The OECT2 device shows a faster turning off in terms of voltage, and the lower On-current (I_{On}) is combined with a lower Off-current (I_{Off}). The transconductance (Fig. 4.31), which is of the order of millisiemens, slightly decreased but remains consistent.

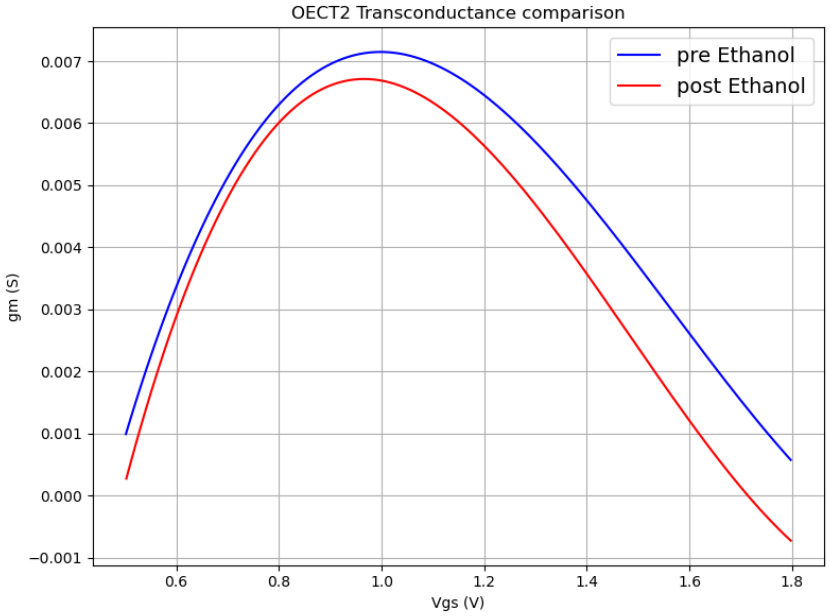

Figure 4.31: OECT2 transconductance comparison before and after the ethanol sterilisation.

The device stability in PBS was then tested by leaving the OECT2 immersed in PBS for several days. The transfer characteristics and transconductance plots obtained during the testing period are shown in Figs. 4.32 and 4.33.

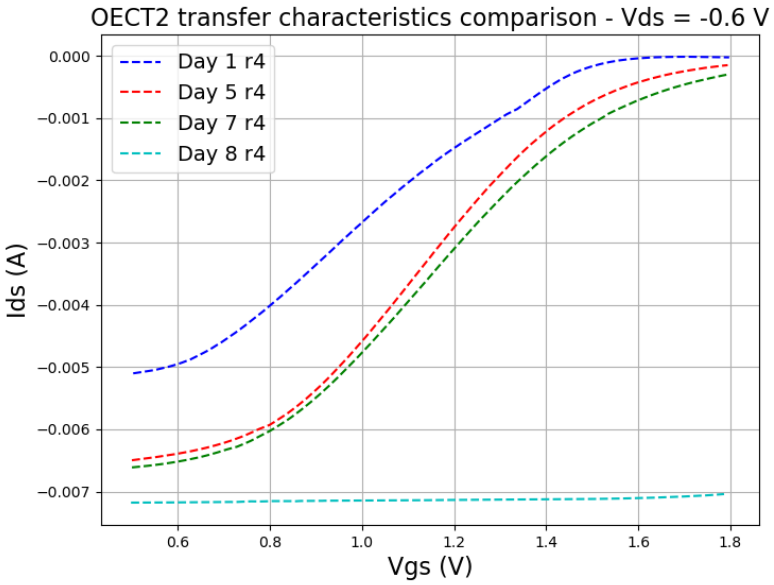

Figure 4.32: OECT2 transfer characteristic comparison during the stability testing period.

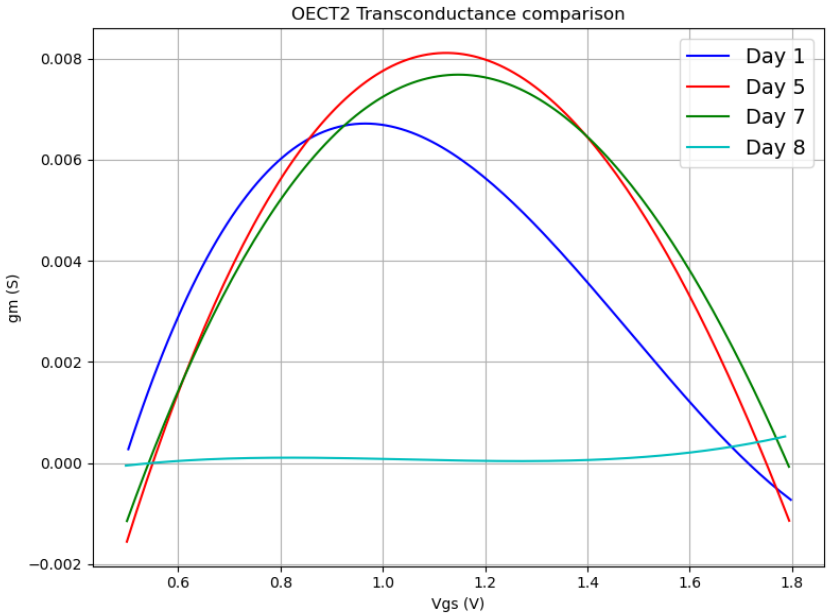

Figure 4.33: OECT2 transconductance comparison during the stability testing period.

It can be noticed that the device operation remained more or less coherent until the seventh day, despite a partial worsening of its turning off. However, after the eighth day, the device stopped working.

The reason behind the device breakdown is most likely the corrosion of the gate electrode caused by the high voltages involved in the electrical characterisation. As a consequence, the gating effect is no longer efficient, and the PEDOT:PSS channel is not being dedoped. This would explain the device not turning off after the eighth day.
Therefore, the device malfunction might not have been caused by poor stability in PBS and a more extensive analysis would be needed to better understand the real device stability in long time ranges, using a more reliable PEDOT:PSS deposition method that allows the OECT to turn off within a narrower voltage range.

A second set of three devices was prepared, always using manual dropcasting to deposit the PEDOT:PSS channel, to test device resistance to autoclave sterilisation. The three devices were first characterised and their transfer characteristic and transconductance were obtained (Figs. 4.34 and 4.35). The comparison of their characteristics shows that deposition by dropcasting does not deliver good reproducibility, as the three devices have different behaviours. OECT5 in particular has an anomalous behaviour in the low voltage part of the transfer characteristic, since an increase of the current is not expected when increasing the gate voltage; furthermore, the device turning off is also not as good as the other two devices.
Nevertheless, as mentioned, this analysis does not aspire to be accurate and rigorous, given the unreliability of the deposition process, but rather a first general analysis to verify the device stability.

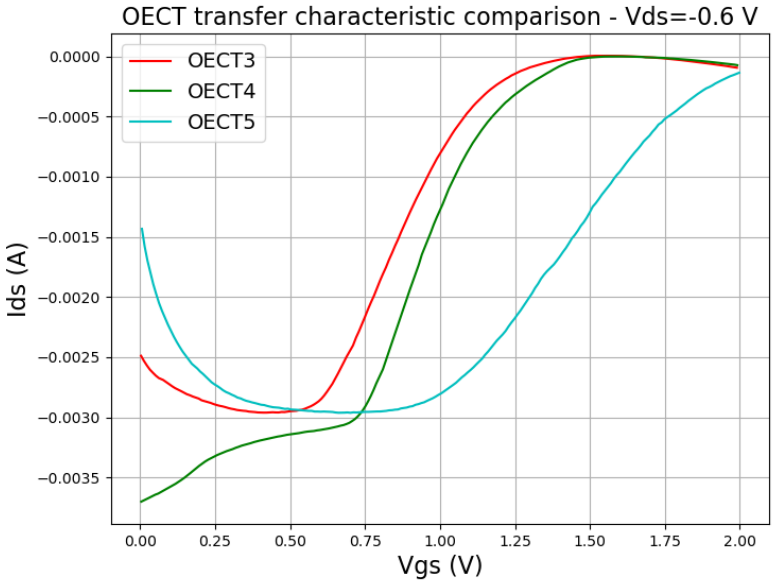

Figure 4.34: OECT3, OECT4 and OECT5 transfer characteristic comparison.

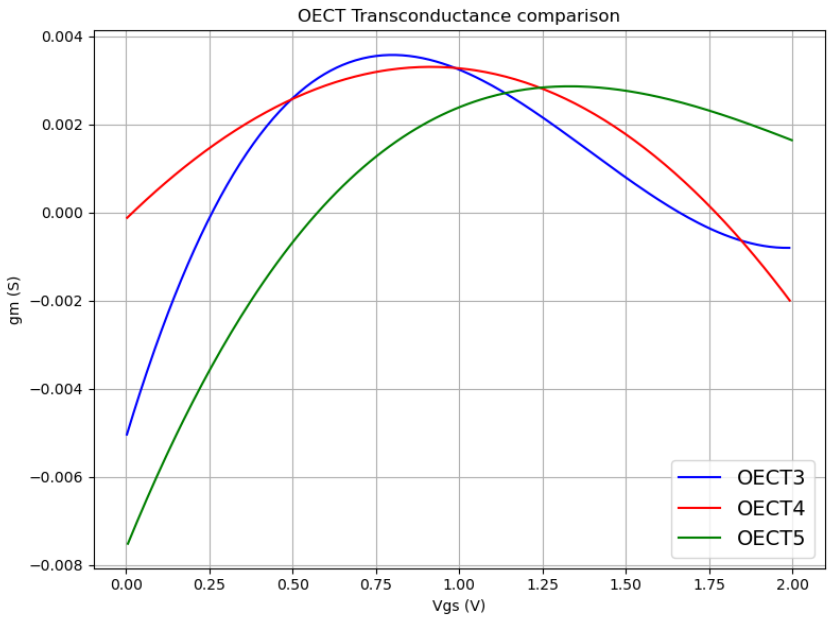

Figure 4.35: OECT3, OECT4 and OECT5 transconductance comparison.

The tree devices were then sterilised in an autoclave. The transfer characteristic was measured to observe the occurrence of any variations following the sterilisation process. The obtained results are presented in Figs. 4.36, 4.37 and 4.38.

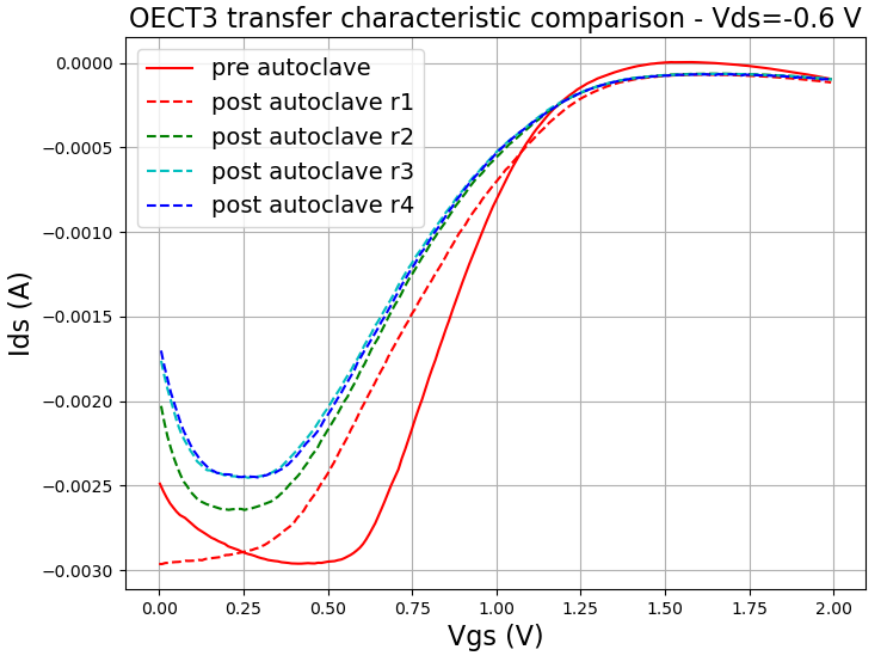

Figure 4.36: OECT3 transfer characteristic comparison before and after autoclave sterilisation.

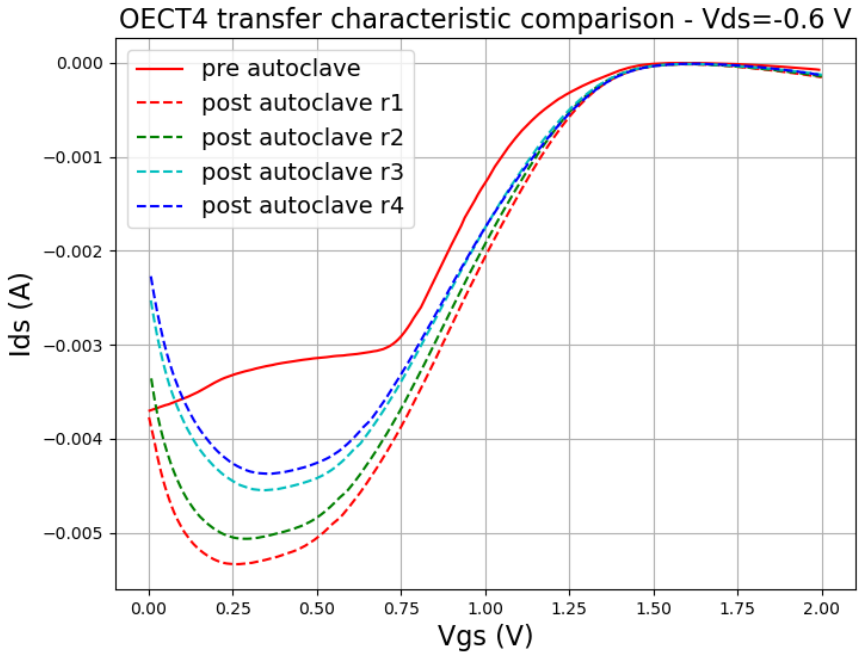

Figure 4.37: OECT4 transfer characteristic comparison before and after autoclave sterilisation.

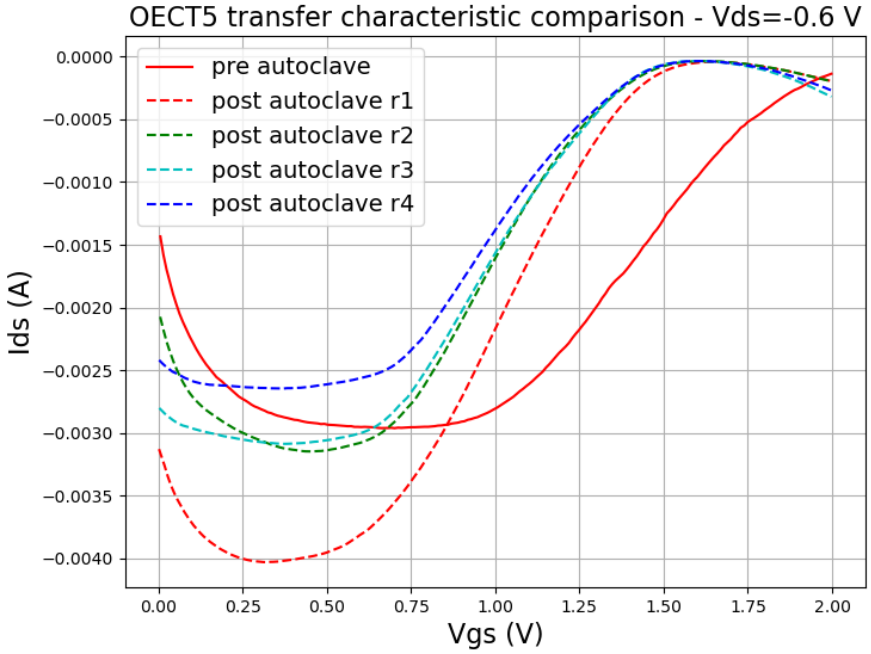

Figure 4.38: OECT5 transfer characteristic comparison before and after autoclave sterilisation.

The curves show that autoclave sterilisation slightly changes the currents involved in the device operation, but overall the trend seems to be that of an OECT. However, the increasing repetitions show a gradual decrease of the transfer characteristic curve.

This may suggest a partial degradation of the device performance, and this is indeed the case after further repetitions. The reasons behind this degeneracy of the device operation have to be addressed, in order to understand if it is linked to the autoclave sterilisation or simply to the high voltages involved in the characterisation process. A possible explanation is a combination of the two things, since the high voltages may cause the degradation of the gold electrodes, while the autoclave sterilisation might be linked to a partial delamination of the PEDOT:PSS channel.

4.4 Caco-2 cell line barrier integrity analysis

The analysis of the cell growth and barrier integrity of a Caco-2 cellular monolayer was performed using the device in the amperometric configuration, as briefly explained in section 3.4. A square wave voltage is periodically applied between the two gate electrodes (Top and Bottom) of each well and the transient current response is measured with a sampling rate of 2.5 ms. The obtained current values are collected and then fitted with a decreasing exponential model.

This approach is based on a simplified version of the equivalent electric circuit proposed in the literature to model epithelial and endothelial cells monolayers [32][33][34]. In particular, the Caco-2 cellular membrane is here modelled as a resistor in parallel with a capacitor, thus forming an RC circuit. The resistance corresponds to the TEER of the cell layer, taking into account the contributions of the flow of current through the intercellular clefts. It reflects how tightly the cells are joined, so that a higher R corresponds to tighter cells, while a lower R is linked to a leaky barrier. The transcellular pathway, that considers the contribution of the current flowing across the cells, is represented by the electrical capacitance [32]. As a consequence, the current values are fitted using the transient response of an RC circuit, using the following equation:

$$I_t = a \cdot e^{-\frac{t}{b}} + cc \tag{4.1}$$

For each curve, these three parameters were derived:

- a is the peak value of the current at $t = 0$, when the voltage step is applied;
- b is the time constant of the circuit ($\tau = RC$);
- cc is the background noise of the collected data.

The most relevant parameter is b, since it is better suited to monitor over time the cell growth and the integrity of the barrier. Indeed, a higher time constant corresponds to a slower decay of the transient current, and this may be linked either to a stronger barrier with a good integrity of the junctions (higher R) or to larger and intact cells that store charge longer (higher C).
The analysis focused on the monitoring of the temporal trend of the b parameter. Specifically, a mean value of the parameter is calculated from the data obtained

over a 10-minute measurement interval. The different average values are plotted, to obtain the trend over time of the b parameter.

Three wells (C1, A4, B4) with a Caco-2 barrier were analysed, while a fourth one (C4) was used as a reference well, in which only the medium was present.
The curves obtained are presented below, with a confidence interval of 95%.

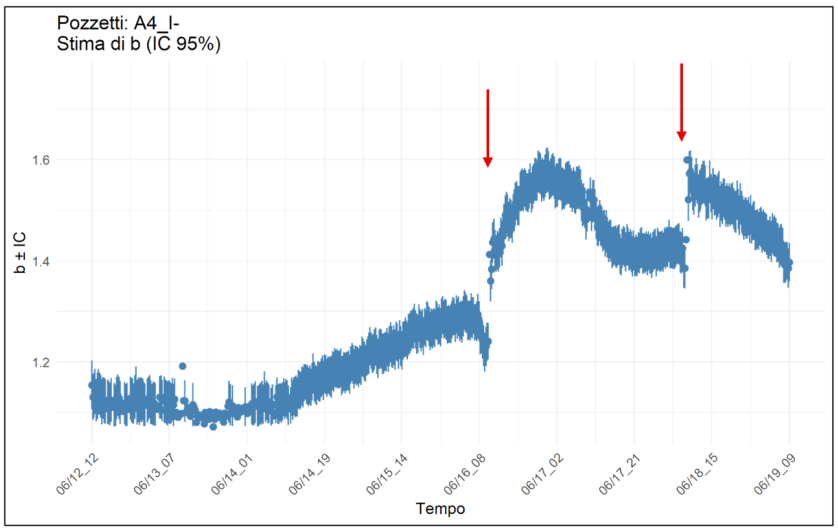

Figure 4.39: Trend over time of the b parameter for the A4 well under a negative square wave voltage (V=-0.5 V). Red arrows indicate a change of the culture medium.

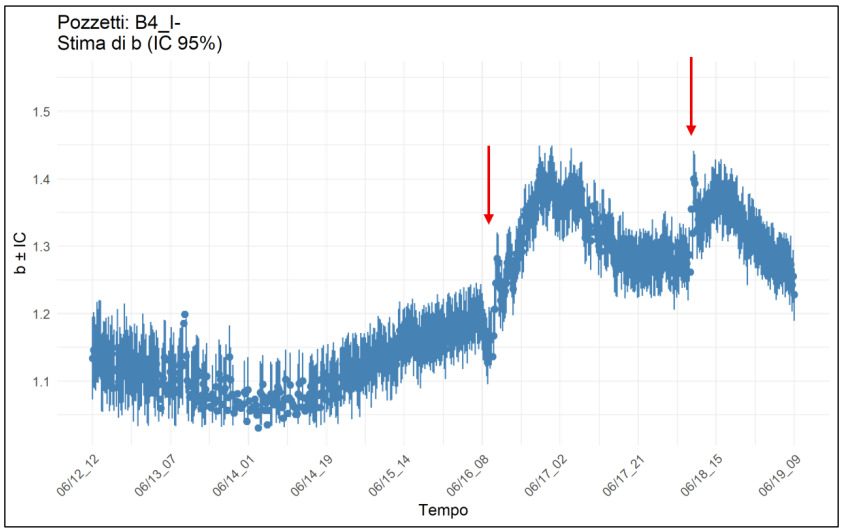

Figure 4.40: Trend over time of the b parameter for the B4 well under a negative square wave voltage (V=-0.5 V). Red arrows indicate a change of the culture medium.

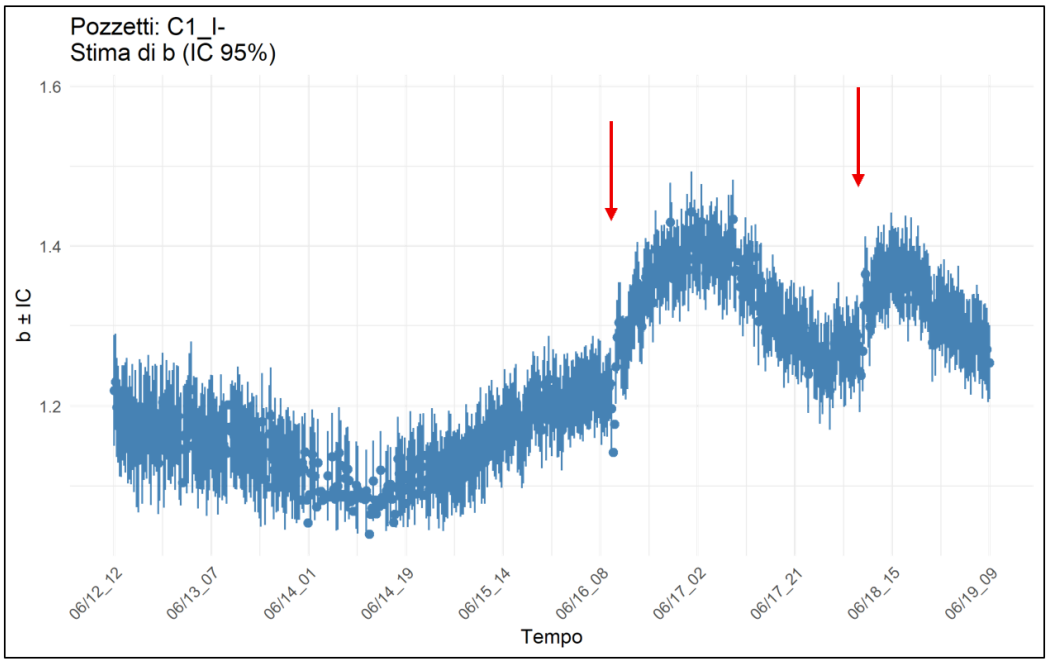

Figure 4.41: Trend over time of the b parameter for the C1 well under a negative square wave voltage (V=-0.5 V). Red arrows indicate a change of the culture medium.

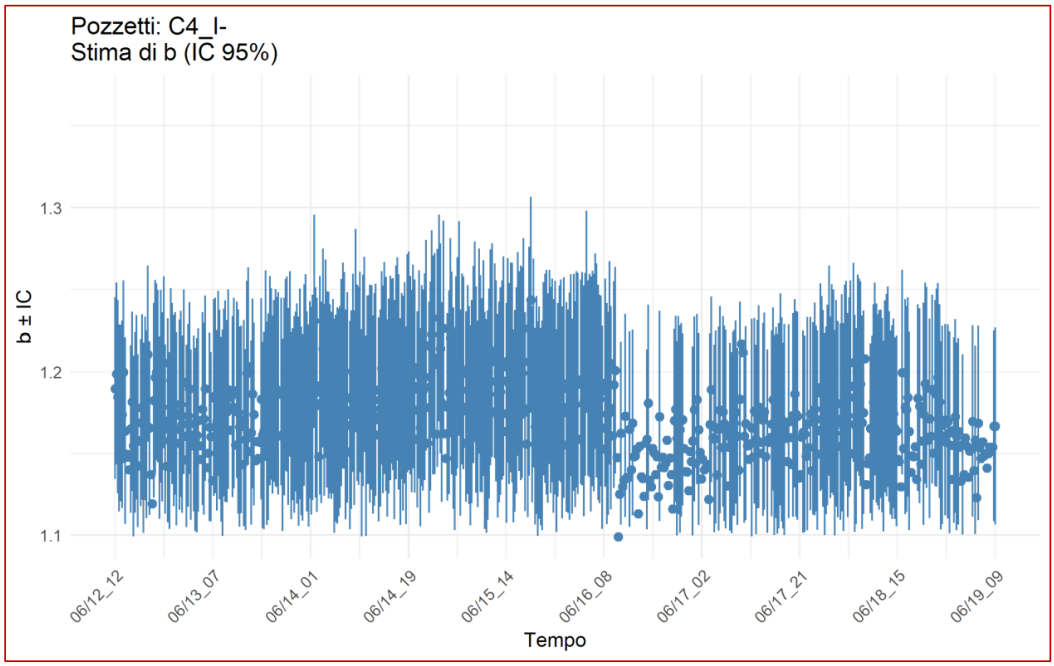

Figure 4.42: Trend over time of the b parameter for the C4 well under a negative square wave voltage (V=-0.5 V).

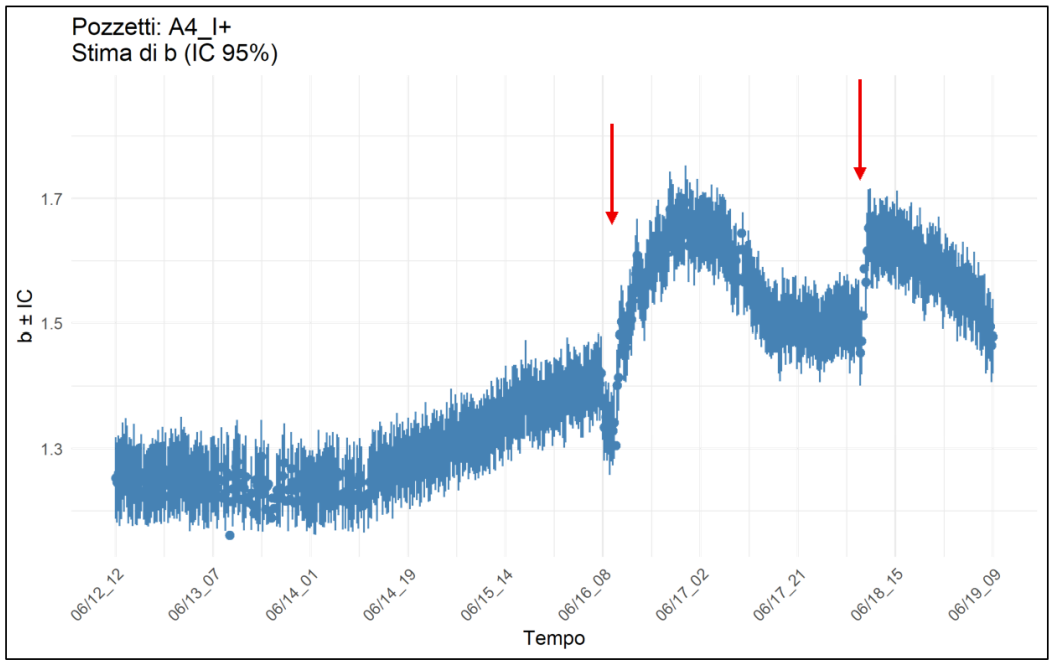

Figure 4.43: Trend over time of the b parameter for the A4 well under a positive square wave voltage (V=0.5 V). Red arrows indicate a change of the culture medium.

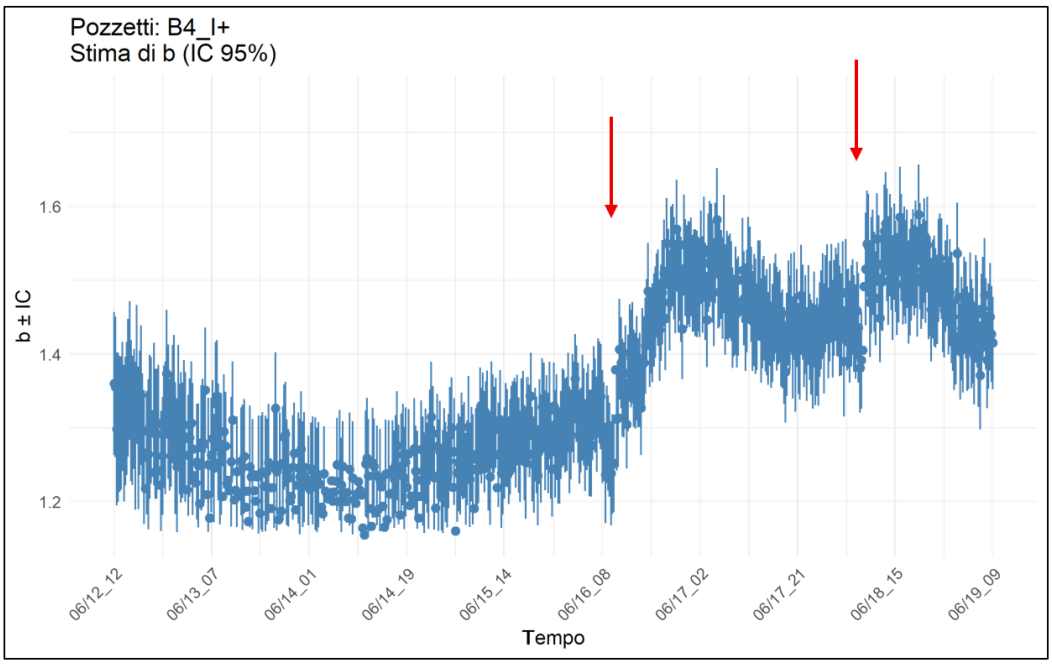

Figure 4.44: Trend over time of the b parameter for the B4 well under a positive square wave voltage (V=0.5 V). Red arrows indicate a change of the culture medium.

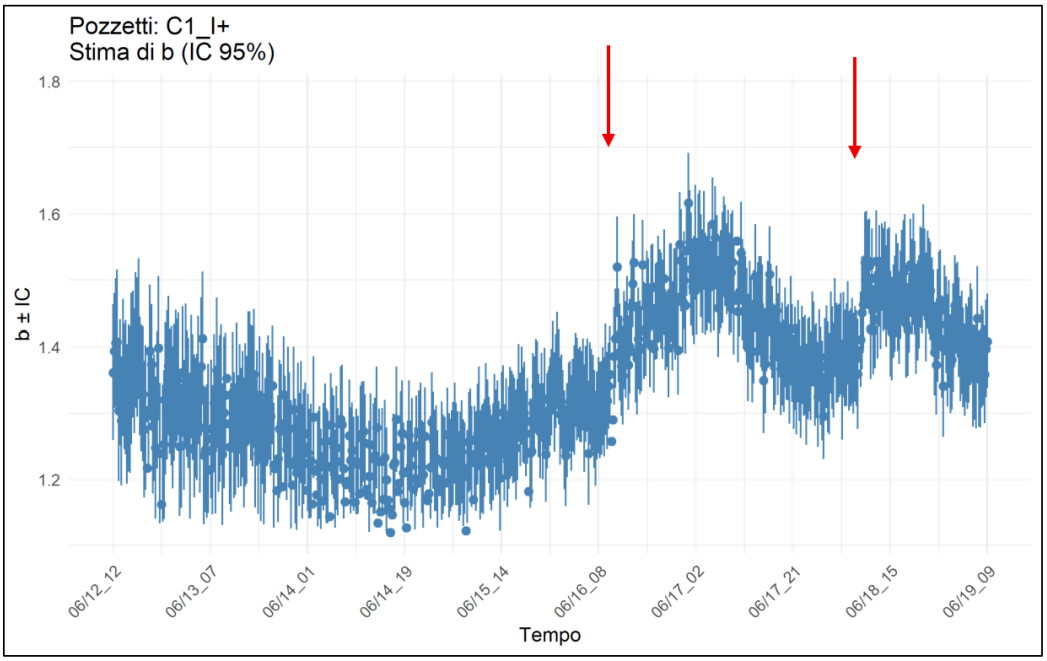

Figure 4.45: Trend over time of the b parameter for the C1 well under a positive square wave voltage (V=0.5 V). Red arrows indicate a change of the culture medium.

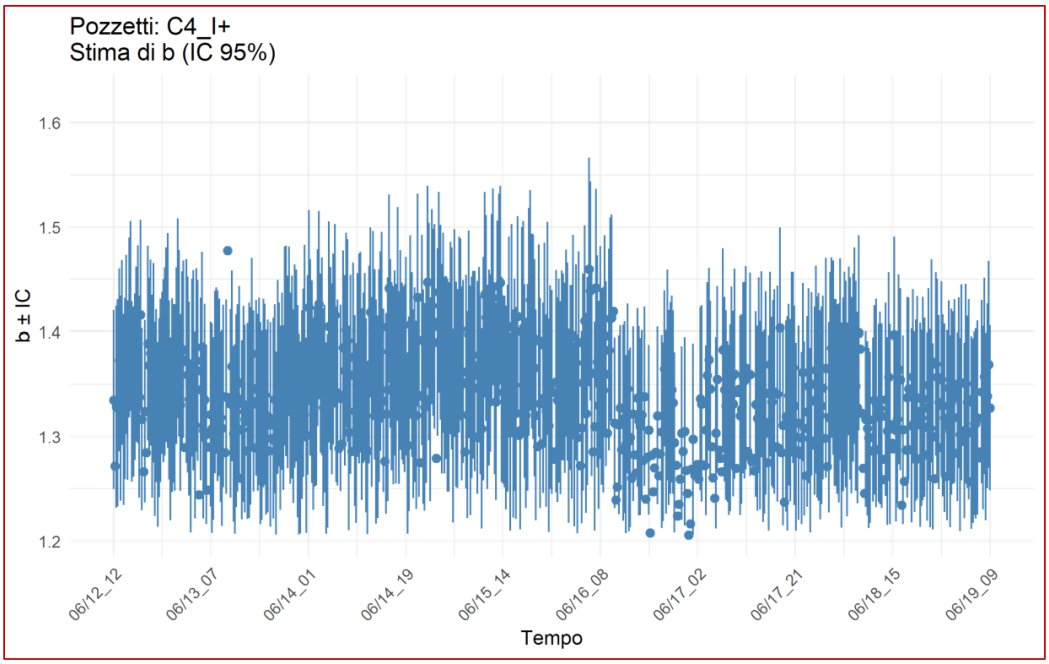

Figure 4.46: Trend over time of the b parameter for the C4 well under a positive square wave voltage (V=0.5 V).

The b parameter in the wells where Caco-2 cells were seeded (Figs. 4.39, 4.40, 4.41, 4.43, 4.44, 4.45) shows an increasing trend over time. This behaviour is reasonable, since it is consistent with an increase of the resistance, and thus of the barrier integrity, as the cellular barrier proceeds to form on the permeable membrane of the transwell insert.

On the other hand, in the well with only the culture medium, where the Caco-2 cells were not seeded, the b parameter is mostly constant in time (Figs. 4.42 and 4.46), and its value is coherent with the initial values of the parameter in the other three wells, when the barrier had not formed yet.
It is possible to notice that simultaneously with the culture medium change, a steep increase of the b parameter occurs, as indicated by the red arrows in the plots. The reasons behind this behaviour might be several, such as the different temperature or pH of the new medium, or the lower ionic strength with respect to the replaced one. Otherwise, the medium change might cause the removal of some metabolites and waste products that weakened the junctions between cells, and the introduction of other substances that favor the maintenance of these cell junctions.
Overall, the analysis gave some reasonable results, coherent with the expectations.

Chapter 5

Conclusion and perspectives

This thesis work focused on the design and fabrication of a biosensing platform capable of continuously monitoring an in vitro-grown cell barrier. A first device was fabricated implementing the original design, which showed good results in terms of integration on the multi-well plate and manageability. An alternative device design was also proposed which presented some optimizations and aimed to simplify the fabrication steps. The fabrication process was adapted to the new layout and the final device showed good results as well.
Different techniques were investigated for the deposition of PEDOT:PSS on the OECT channel. Manual deposition through drop-casting was adopted, despite the drawback of low reproducibility that introduces sample-to-sample variability. The transistors were then electrically characterised and the main figures of merit were extracted. The transfer characteristics showed coherent values of the On current (I_{on}), transconductance (g_m) and I_{on}/I_{off} ratio. The turning off of the OECTs occurred for higher voltage values compared to the standard ones. The transfer characteristics were used as a reference to compare the performances of the different transistors; the low reproducibility of the PEDOT:PSS deposition is reflected in the differences that emerged in the comparison.
The device stability over time was tested in PBS for few days. A degradation of the performance was observed after the eighth day, suggesting that the use of high voltages is detrimental for the gold electrodes.
In order to verify the compatibility of the device with the most common sterilisation processes, the OECTs were characterised both after bathing in a 70% ethanol in water solution and after autoclave sterilisation.
The biocompatibility of the system was addressed by leaving the device in an incubator with a culture medium. No contamination was detected after four days.
A Caco-2 cellular barrier was analysed using the device in the amperometric configuration. The results showed promising results in the continuous monitoring of the barrier integrity.

Future improvements might address the PEDOT:PSS deposition, considering the adoption of more reliable techniques, which allow for reproducibility and a stronger

adhesion to the substrate. An investigation of possible optimizations that could yield a better performance of the OECTs would also be beneficial. In particular, achieving a faster turn-off of the devices in terms of voltage range would be optimal. The different measurement setups available due to the device layout should be explored. Further analysis can be conducted on different cell lines to understand the potentiality of the device. Finally, it would be useful to compare the results obtained with those from standard methods, in order to validate them.

Bibliography

[1] Henry S White, Gregg P Kittlesen, and Mark S Wrighton. "Chemical derivatization of an array of three gold microelectrodes with polypyrrole: fabrication of a molecule-based transistor". In: *Journal of the American Chemical Society* 106.18 (1984), pp. 5375–5377 (cit. on p. 3).

[2] David Ohayon, Victor Druet, and Sahika Inal. "A guide for the characterization of organic electrochemical transistors and channel materials". In: *Chemical Society Reviews* 52.3 (2023), pp. 1001–1023 (cit. on pp. 3, 4, 8–10, 12, 16, 34).

[3] Hong Liu, Jiajun Song, Zeyu Zhao, Sanqing Zhao, Zhiyuan Tian, and Feng Yan. "Organic electrochemical transistors for biomarker detections". In: *Advanced Science* 11.27 (2024), p. 2305347 (cit. on p. 4).

[4] Jonathan Rivnay, Sahika Inal, Alberto Salleo, Róisín M Owens, Magnus Berggren, and George G Malliaras. "Organic electrochemical transistors". In: *Nature Reviews Materials* 3.2 (2018), pp. 1–14 (cit. on pp. 4, 8, 12, 16).

[5] Thanh-Hai Le, Yukyung Kim, and Hyeonseok Yoon. "Electrical and electrochemical properties of conducting polymers". In: *Polymers* 9.4 (2017), p. 150 (cit. on pp. 4–6).

[6] Md Byzed Hasan, Md Masud Parvez, Abrar Yasir Abir, and Md Faruak Ahmad. "A Review on Conducting Organic Polymers: Concepts, Applications, and Potential Environmental Benefits". In: *Heliyon* (2025) (cit. on pp. 5, 6).

[7] Zeng Fan and Jianyong Ouyang. "Thermoelectric properties of PEDOT: PSS". In: *Advanced Electronic Materials* 5.11 (2019), p. 1800769 (cit. on p. 7).

[8] Charalampos Pitsalidis et al. "Organic bioelectronics for in vitro systems". In: *Chemical Reviews* 122.4 (2021), pp. 4700–4790 (cit. on p. 7).

[9] K Namsheer and Chandra Sekhar Rout. "Conducting polymers: a comprehensive review on recent advances in synthesis, properties and applications". In: *RSC advances* 11.10 (2021), pp. 5659–5697 (cit. on p. 8).

[10] Jacob T Friedlein, Robert R McLeod, and Jonathan Rivnay. "Device physics of organic electrochemical transistors". In: *Organic Electronics* 63 (2018), pp. 398–414 (cit. on p. 8).

[11] Daniel A Bernards and George G Malliaras. "Steady-state and transient behavior of organic electrochemical transistors". In: *Advanced Functional Materials* 17.17 (2007), pp. 3538–3544 (cit. on pp. 10–12).

[12] RS. *RS PRO 37-way flat ribbon cable Datasheet*. URL: https://docs.rs-online.com/de75/A700000008750121.pdf (cit. on p. 18).

[13] RS. *RS Pro 37-Way IDC D-sub Connector Datasheet - Socket*. URL: https://docs.rs-online.com/679b/0900766b814fdfd0.pdf (cit. on p. 18).

[14] RS. *RS Pro 37-Way IDC D-sub Connector Datasheet - Plug*. URL: https://docs.rs-online.com/b505/0900766b81581c21.pdf (cit. on p. 18).

[15] DuPont^{TM}. *Kapton HN polyimide film Datasheet*. URL: https://www.dupont.com/content/dam/electronics/amer/us/en/electronics/public/documents/en/EI-10206-Kapton-HN-Data-Sheet.pdf (cit. on p. 22).

[16] Inês Miranda, Andrews Souza, Paulo Sousa, João Ribeiro, Elisabete MS Castanheira, Rui Lima, and Graça Minas. "Properties and applications of PDMS for biomedical engineering: A review". In: *Journal of functional biomaterials* 13.1 (2021), p. 2 (cit. on p. 22).

[17] DOW. *Sylgard^{TM}184SiliconeElastomerTechnicalDatasheet*. URL: https://www.dow.com/documents/11/11-3184-01-sylgard-184-elastomer.pdf (cit. on p. 22).

[18] Younan Xia and George M Whitesides. "Soft lithography". In: *Angewandte Chemie International Edition* 37.5 (1998), pp. 550–575 (cit. on pp. 23, 24).

[19] Stefania Torino, Laura Conte, Mario Iodice, Giuseppe Coppola, and Ralf D Prien. "PDMS membranes as sensing element in optical sensors for gas detection in water". In: *Sensing and bio-sensing research* 16 (2017), pp. 74–78 (cit. on p. 25).

[20] Nanoscience Instruments. *Profilometry*. URL: https://www.nanoscience.com/techniques/profilometry/#:~:text=Profilometry%20is%20a%20technique%20used,probe%20or%20by%20using%20light. (cit. on pp. 25, 26).

[21] Narendra B Dahotre, Sameer R Paital, Anoop N Samant, and Claus Daniel. "Wetting behaviour of laser synthetic surface microtextures on Ti–6Al–4V for bioapplication". In: *Philosophical Transactions of the Royal Society A: Mathematical, Physical and Engineering Sciences* 368.1917 (2010), pp. 1863–1889 (cit. on p. 28).

[22] Alexandra Borók, Kristóf Laboda, and Attila Bonyár. "PDMS bonding technologies for microfluidic applications: A review". In: *Biosensors* 11.8 (2021), p. 292 (cit. on pp. 28, 29).

[23] Shantanu Bhattacharya, Arindom Datta, Jordan M Berg, and Shubhra Gangopadhyay. "Studies on surface wettability of poly (dimethyl) siloxane (PDMS) and glass under oxygen-plasma treatment and correlation with bond strength". In: *Journal of microelectromechanical systems* 14.3 (2005), pp. 590–597 (cit. on p. 28).

[24] Ramakrishna Vasireddi. "Fabrication of Novel Microfluidic Devices for Investigating Ultrafast Structural Dynamics". PhD thesis. Staats-und Universitätsbibliothek Hamburg Carl von Ossietzky, 2019 (cit. on p. 29).

[25] NanoScience Instruments. *Preparing Powders for Scanning Electron Microscopy*. URL: https://www.nanoscience.com/applications/preparing-powders-for-scanning-electron-microscopy/ (cit. on p. 31).

[26] RS. *Silver conductive paint Datasheet*. URL: https://docs.rs-online.com/cd63/A700000008879603.pdf (cit. on p. 31).

[27] RS. *RS PRO Amber Epoxy Potting Compound Technical Data Sheet*. URL: https://docs.rs-online.com/3543/0900766b81580057.pdf (cit. on p. 32).

[28] Stratasys. *PolyJet^{TM}Technology*. URL: https://www.stratasys.com/en/guide-to-3d-printing/technologies-and-materials/polyjet-technology/ (cit. on p. 32).

[29] Aroha B. Sánchez, Ana C. Calpena, Mireia Mallandrich, and Beatriz Clares. "Validation of an ex vivo permeation method for the intestinal permeability of different BCS drugs and its correlation with Caco-2 in vitro experiments". In: *Pharmaceutics* 11.12 (2019), p. 638 (cit. on pp. 35, 36).

[30] Marjon Zamani, Catherine M Klapperich, and Ariel L Furst. "Recent advances in gold electrode fabrication for low-resource setting biosensing". In: *Lab on a Chip* 23.5 (2023), pp. 1410–1419 (cit. on p. 38).

[31] Hyung-Kew Lee, Sun-Il Chang, and Euisik Yoon. "A flexible polymer tactile sensor: Fabrication and modular expandability for large area deployment". In: *Journal of microelectromechanical systems* 15.6 (2006), pp. 1681–1686 (cit. on pp. 41, 42).

[32] Kathrin Benson, Sandra Cramer, and Hans-Joachim Galla. "Impedance-based cell monitoring: barrier properties and beyond". In: *Fluids and Barriers of the CNS* 10 (2013), pp. 1–11 (cit. on p. 63).

[33] Balaji Srinivasan, Aditya Reddy Kolli, Mandy Brigitte Esch, Hasan Erbil Abaci, Michael L Shuler, and James J Hickman. "TEER measurement techniques for in vitro barrier model systems". In: *Journal of laboratory automation* 20.2 (2015), pp. 107–126 (cit. on p. 63).

[34] Francesco Decataldo, Marianna Barbalinardo, Marta Tessarolo, Vito Vurro, Maria Calienni, Denis Gentili, Francesco Valle, Massimiliano Cavallini, and Beatrice Fraboni. "Organic electrochemical transistors: smart devices for real-time monitoring of cellular vitality". In: *Advanced Materials Technologies* 4.9 (2019), p. 1900207 (cit. on p. 63).